

**Correlation of <sup>68</sup>Ga-FAPi-46 PET biodistribution with FAP expression by immunohistochemistry in patients with solid cancers: a prospective translational exploratory study**

Christine E. Mona<sup>1,2,3</sup>, Matthias R. Benz<sup>1,2</sup>, Firas Hikmat<sup>1</sup>, Tristan R. Grogan<sup>4</sup>, Katharina Lueckerath<sup>1,2,3</sup>, Aria Razmaria<sup>1</sup>, Rana Riahi<sup>5</sup>, Roger Slavik<sup>1</sup>, Mark D. Girgis<sup>6</sup>, Giuseppe Carlucci<sup>1</sup>, Kimberly A. Kelly<sup>7</sup>, Samuel W. French<sup>2,5</sup>, Johannes Czernin<sup>1,2,3</sup>, David W. Dawson<sup>#2,5</sup> & Jeremie Calais<sup>#1,2,3</sup>

<sup>1</sup>Ahmanson Translational Theranostics Division, Department of Molecular and Medical Pharmacology, David Geffen School of Medicine, University of California - Los Angeles, Los Angeles, CA, USA

<sup>2</sup>Jonsson Comprehensive Cancer Center, University of California - Los Angeles, Los Angeles CA, USA

<sup>3</sup>Institute of Urologic Oncology, University of California - Los Angeles, Los Angeles, CA, USA

<sup>4</sup>Department of Medicine Statistics Core, David Geffen School of Medicine, University of California - Los Angeles, Los Angeles, CA 90095, USA.

<sup>5</sup>Department of Pathology and Laboratory Medicine, David Geffen School of Medicine, University of California - Los Angeles, Los Angeles, CA, USA

<sup>6</sup>Department of Surgery, Division of Surgical Oncology, David Geffen School of Medicine, University of California - Los Angeles, Los Angeles, CA, USA

<sup>7</sup>Department of Biomedical Engineering, University of Virginia School of Engineering and Applied Sciences; Robert M. Berne Cardiovascular Research Center, University of Virginia School of Medicine, Charlottesville, VA, USA

#These authors contributed equally

**Correspondence to:**

*Jeremie Calais*, MD, MSc

Ahmanson Translational Theranostics Division  
Department of Molecular and Medical Pharmacology  
David Geffen School of Medicine  
University of California Los Angeles  
200 Medical Plaza, Suite B114-61, Los Angeles, CA 90095-7370  
Email: [jcalais@mednet.ucla.edu](mailto:jcalais@mednet.ucla.edu)  
Phone: (310) 825 3617  
Fax: (310) 206 5543

*Christine E. Mona*, PhD

Ahmanson Translational Theranostics Division  
Department of Molecular and Medical Pharmacology  
David Geffen School of Medicine  
University of California Los Angeles  
650 Charles E. Young Drive South, Los Angeles, CA 90095-7370  
Email: [cmona@mednet.ucla.edu](mailto:cmona@mednet.ucla.edu)  
Phone: (310) 206 5459  
Fax: (310) 206 5543

**Running title:** Correlation of FAPi PET and FAP IHC

**Keywords:** Cancer; PET/CT; Fibroblast Activation Protein; Immunohistochemistry; <sup>68</sup>Ga-FAPi-46.

## ABSTRACT

**Purpose:** Fibroblast activation protein (FAP)-expressing cancer-associated fibroblasts confer treatment resistance, promote metastasis and immunosuppression. Because FAP is overexpressed in many cancers, radiolabeled molecules targeting FAP are studied for their use as pan-cancer theranostic agents. This study aims to establish the spectrum of FAP expression across various cancers by immunohistochemistry and to explore whether gallium-68 FAPi-46 ( $^{68}\text{Ga}$ -FAPi-46) PET biodistribution faithfully reflects FAP expression from resected cancer and non-cancer specimens.

**Methods:** We conducted a FAP expression screening by using immunohistochemistry on a pan-cancer human tissue microarray (TMA) (141 patients, 14 different types of cancer) and an interim analysis of a prospective exploratory imaging trial in cancer patients. Volunteer patients underwent one whole body  $^{68}\text{Ga}$ -FAPi-46 PET/CT scan and subsequently, surgical resection of their primary tumor and/or metastasis.  $^{68}\text{Ga}$ -FAPi-46 PET maximum standardized uptake value (SUV<sub>max</sub> and SUV<sub>mean</sub>) was correlated with FAP immunohistochemistry score in cancer and non-cancer tissues for each patient.

**Results:** FAP was expressed across all 14 cancers types on TMA with variable intensity and frequency, ranging from 25 to 100% (mean  $76.6 \pm 25.3\%$ ). Strong FAP expression was observed in 50-100% of cancers of the bile duct, bladder, colon, esophagus, stomach, lung, oropharynx, ovary and pancreas. Fifteen patients with various cancer types (colorectal (n=4), head and neck (n=3), pancreas (n=2), breast (n=2), stomach (n=1), esophagus (n=2) and uterus (n=1)) underwent surgery following their  $^{68}\text{Ga}$ -FAPi-46 PET/CT scan within a mean time interval of  $16.1 \pm 14.4$  days.  $^{68}\text{Ga}$ -FAPi-46 SUVs and immunohistochemistry scores were higher in cancer than in normal tissue: mean SUV<sub>max</sub> 7.7 vs 1.6 ( $p < 0.001$ ), mean SUV<sub>mean</sub> 6.2 vs 1.0 ( $p < 0.001$ ) and mean FAP immunohistochemistry score 2.8 vs 0.9 ( $p < 0.001$ ). FAP immunohistochemistry scores strongly correlated with  $^{68}\text{Ga}$ -FAPi 46 SUV<sub>max</sub> and SUV<sub>mean</sub>:  $r = 0.781$  (95%CI 0.376-0.936;  $p < 0.001$ ) and  $r = 0.783$  (95%CI 0.379-0.936;  $p < 0.001$ ), respectively.

**Conclusion:** In this interim analysis of a prospective exploratory imaging trial,  $^{68}\text{Ga}$ -FAPi-46 PET biodistribution across multiple cancers strongly correlated with FAP tissue expression. These findings support further exploration of FAPi PET as a pan-cancer imaging biomarker for FAP expression and stratification tool for FAP- targeted therapies.

## **INTRODUCTION**

Fibroblast activation protein (FAP) is highly expressed on cancer-associated fibroblasts and is a key player in tumor progression (1). High FAP expression is almost exclusively restricted to cancer-associated fibroblasts and serves as an independent negative prognostic factor for multiple types of cancers (2). *In vivo* depletion of FAP-positive stromal cells inhibits tumor growth by decreasing cancer support, increasing anti-tumor immunity and limiting stromal barrier effects (3-5). However, targeting the enzymatic activity of FAP with antibodies does not yield beneficial clinical effects (6,7). Recently, FAP-targeting ligands (FAPi) labeled with Positron Emission Tomography (PET) imaging (e.g., Gallium-68, Fluor-18 for Positron Emission Tomography; PET) and therapeutic (e.g., Lutetium-177, Yttrium-90) radioisotopes have been introduced (8,9). High tumor uptake observed with FAPi PET imaging in various cancers suggests promising potential of radiolabeled FAPi compounds for diagnostic and therapeutic applications (10).

In this translational prospective exploratory study, we aimed at assessing the utility of FAPi PET imaging as a pan-cancer imaging biomarker for FAP expression. We first surveyed tissue microarrays (TMAs) of 141 patients with 14 cancer types for presence and degree of FAP expression by immunohistochemistry (11). A cohort of surgical patients representing 10 of those cancer types was then tested to determine the correlation between <sup>68</sup>Ga-FAPi-46 PET biodistribution and FAP immunohistochemistry expression in excised tumor tissue.

## **METHODS**

### **Tissue Microarray Screening**

FAP expression in human tumor tissue was assessed using a pan-cancer TMA obtained from University of Virginia (KA.K.). This TMA included 141 patients with 14 different types of cancer (bile duct, bladder, breast, colon, esophagus, stomach, liver, lung, ovary, oropharynx, pancreas, prostate, kidney, and uterus; 6 to 14 tumors per tissue type). Normal tissues present on the TMA were also evaluated (5 to 8 samples per tissue type). After deparaffinization and rehydration, heat-induced antigen retrieval (sodium citrate, 0.05% Tween 20, pH 6.0) was performed for 20 minutes using a vegetable steamer followed by quenching of endogenous peroxidase activity (3% hydrogen

peroxide, 10 minutes). Primary antibody incubation with a 1:50 dilution of rabbit monoclonal anti-FAP alpha [EPR20021] (ab207178; Abcam, Cambridge, MA) was performed overnight at 4°C. Detection was performed using the UltraView Universal DAB Detection Kit (DAKO, K3467, Carpinteria, CA) per manufacturer's instructions. An experienced surgical pathologist (DW.D.) confirmed histologic diagnoses and performed analysis of immunohistochemistry using a semi-quantitative scoring system (0= negative, 1= weak, 2= strong staining).

### **Clinical Study Design and Participants**

We conducted a prospective exploratory biodistribution study of <sup>68</sup>Ga-FAPI-46 PET imaging under the Radioactive Drug Research Committee (RDRC) Program (21 CFR 361.1). The primary objective was to define the biodistribution of <sup>68</sup>Ga-FAPi-46 PET in normal and cancer tissues and further correlate with tissue expression as determined by FAP immunohistochemistry. Volunteer cancer patients scheduled to undergo surgical resection of primary tumor and/or metastasis were eligible (inclusion and exclusion criteria in supplemental table 1). The type of surgery depended on the location and disease determined by clinical standard of care explorations. <sup>68</sup>Ga-FAPi-46 PET/computed tomography (CT) imaging findings did not impact the therapy plan and surgery was performed independently of the results of the scan findings. The study was approved by the University of California Los Angeles (UCLA) Institutional Review Board (IRB#19-000756) and registered on ClinicalTrials.gov (NCT04147494). All patients provided oral and written informed consent.

We present here the results of an interim analysis that was mandated by the UCLA Jonsson Comprehensive Cancer Center (JCCC) Internal Scientific Peer Review Committee (ISPRC) and Data Safety Monitoring Board (DSMB) after completed enrollment of 15 patients.

### **FAPi PET/CT Image Acquisition**

<sup>68</sup>Ga-FAPi-46 was used as the FAP-targeted radioligand (8). The mean injected activity was 184±3 MBq (range, 174 – 185MBq). The mean uptake time was 63±10 minutes (range, 54 – 96 minutes). Images were acquired using 64-detector PET/CT

scanners (Biograph 64 mCT (n=7) or Biograph 64 TruePoint (n=8), Siemens Healthcare, Erlangen, Germany). A non-contrast CT (120 kV, 80 mAs) was performed for attenuation correction and anatomic correlation of the PET findings. PET images were acquired from vertex to mid-thigh, using an emission time of 2-4 minutes per bed position, depending on patient body weight. All PET images were reconstructed using correction for attenuation, dead time, random events, and scatter. PET images were reconstructed using an iterative algorithm (ordered-subset expectation maximization).

### **FAPi PET/CT Image Analysis**

Images were analyzed in consensus by two readers (J.Ca., MR.B.) blinded to the histopathology and immunohistochemistry results. The readers had access to all medical records and other imaging modality available to facilitate tumor localization. OsiriX DICOM viewer (Pixmeo, Switzerland) was used (12). Readers quantified the <sup>68</sup>Ga-FAPi-46 PET uptake in cancer tissue and non-cancer tissue by placing volumes of interest (VOI) in the tumor lesion(s) and the surrounding normal tissue in the same organ. Readers adapted the size of the VOI visually to best encompass the structure of interest and to preclude overlapping activity between the cancer and non-cancer VOIs. Anatomic CT information was used to avoid activity spillover from other organs. Mean and maximum standardized uptake values (SUV<sub>mean</sub> and SUV<sub>max</sub>) and lesion size by CT were recorded.

### **Histopathology and Immunohistochemistry Analysis**

Clinical pathology reports were used to collect final pathology diagnoses and pathologic TNM staging. Representative normal and tumor tissue sections from surgical resection specimens were obtained from the UCLA Department of Pathology through the UCLA Translational Pathology Core Laboratory (TPCL). FAP immunohistochemistry staining was performed as described above.

An evaluation of all H&E slides from each surgical pathology case was performed (DW.D.) to select representative sections of normal and tumor tissue for immunohistochemistry evaluation. One representative section that best reflected the

overall tumor histology (i.e. histologic type and grade, relative stroma and tumor cell component), that included sampling of both the edge and the central portions of the tumor mass, and that contained surrounding adjacent normal tissue (>5mm distance from malignant cells) was selected for each patient. Immunohistochemistry stains were independently scored by two pathologists (DW.D., SW.F.) who were blinded to each other's scoring, clinical information and PET imaging results. A semi-quantitative approach adapted from a prior study was used (13). Briefly, FAP expression was assessed globally across the entire cross-sectional area of tumor and adjacent non-malignant tissue without any specific focus on invasive fronts or areas of active tumor growth. The tumor compartment was defined based on morphologic assessments as the geographic area where malignant cells were present, as well as the immediately adjacent area of intratumoral and peritumoral stromal response. Score 0 was defined as complete absence of staining or weak staining in <10% of area under assessment. Score 1 was defined weak expression in greater than 10% of area under assessment. Score 2 was defined as moderate or strong expression in 10-50% of area under assessment. Score 3 was defined as moderate or strong expression in >50% of area under assessment.

### **Cross-Sectional Correlation Analysis of the FAPi PET Signal and FAP Immunohistochemistry Staining**

The <sup>68</sup>Ga-FAPi-46 PET SUV and the FAP immunohistochemistry score of cancer and non-cancer tissue were evaluated for correlation on a per-patient basis: for each tumor lesion, the <sup>68</sup>Ga-FAPi-46 PET SUV of the lesion was evaluated for correlation with the immunohistochemistry score of the tumor compartment on the selected pathology slide and the <sup>68</sup>Ga-FAPi-46 PET SUV of the normal tissue surrounding the tumor lesion was evaluated for correlation with the immunohistochemistry score of the non-cancer tissue available on the same pathology slide containing the tumor lesion.

### **Statistics**

Patient characteristics and study variables were summarized using mean, standard deviation, ranges or frequency (%) as appropriate. To test for differences in expression levels of both immunohistochemistry and PET measures between cancer and

non-cancer tissues, the two groups were compared using p-values from a Generalized Estimating Equation (GEE) model (to properly account for the repeated measures design of the study)(14). For assessing the association between immunohistochemistry and PET findings, we computed repeated measures correlation coefficients. Inter-reader agreement for the immunohistochemistry scoring was assessed using Cohen's kappa statistics. P-values <0.05 were considered statistically significant. Analyses were carried out using SAS V9.4 (SAS Institute, Cary, NC) and R V3.6.1 ([www.r-project.org](http://www.r-project.org), Vienna, AU, *Rmcorr package*). Due to the exploratory nature of this study, and the RDRC mandated limit of 30 patients, with an interim analysis after 15 patients mandated by the UCLA IRB, a power analysis for sample size was not performed.

## **RESULTS**

### **Tissue Microarray Analysis**

Representative FAP immunohistochemistry scoring by cancer type performed in the TMA is shown in Figure 1. FAP expression was present in 80.9% (114/141) of tumors. Of the 114 positive tumors, FAP expression was stromal in 108/114, epithelial in 1/114, and mixed in 5/114 of cases (Lung cancer (N=1), Ovarian cancer (N=1), Oropharynx (N=1), Pancreatic (N=1) and Uterine cancer (N=1)). No stroma was present for evaluation in one case of ovarian cancer (0.7%).

While there was variability in the intensity and frequency of FAP expression, FAP was positive in more than 50% of cases from eleven of fourteen cancer types. Strong FAP expression was observed in 50-100% of cancers from the bile duct, bladder, colon, esophagus, stomach, lung, oropharynx, ovary and pancreas. Liver, prostate and renal cell cancer were shown to be the three tumor types with the lowest FAP expression.

This TMA survey provided rationale for the study design of the subsequent clinical PET imaging study.

### **PET Imaging Study Cohort**

Between December 2019 and May 2020, 15 patients (8 men and 7 women; mean age: 60.7 ± 10.5 years) with 7 different cancer types (colorectal (N=4), head and neck (N=3), pancreatic (N=2), breast (N=2), gastric (N=1), esophageal (N=2) and uterine (N=1)



cancer) were enrolled. Supplemental Table 2 summarizes the demographics and clinical characteristics of the study population. All 15 patients underwent a  $^{68}\text{Ga}$ -FAPi-46 PET/CT and subsequently underwent surgery within  $16.1 \pm 14.4$  days (range 1 – 50 days) after the  $^{68}\text{Ga}$ -FAPi-46 PET/CT scan. Two patients had tumors deemed unresectable at the time of surgery (gastric linitis plastica with duodenal extension, patient #003; pancreatic cancer with venous involvement, patient #014).

### **$^{68}\text{Ga}$ -FAPi-46 PET Biodistribution in Cancer and Non-Cancer Tissues**

The  $^{68}\text{Ga}$ -FAPi-46 biodistribution as determined by SUVmean in normal organs is described in Supplemental Table 3 and Supplemental Figure 1. The  $^{68}\text{Ga}$ -FAPi-46 SUVs and the size of the cancer lesions are provided in Supplemental Tables 4 (primary tumors) and 5 (metastases).

*Non-cancer tissues:* The urinary bladder due to urinary excretion and the uterus due to normal myometrial FAP expression showed highest normal organ  $^{68}\text{Ga}$ -FAPi-46 PET signal. Other organs with notable  $^{68}\text{Ga}$ -FAPi-46 uptake included submandibular glands, Waldeyer's ring, pancreas, and kidneys (average SUVmean < 2.5).  $^{68}\text{Ga}$ -FAPi-46 uptake higher than normal tissues was noted in three lesions (SUVmax of 4.4, 2.4 and 2.6) that subsequently revealed benign pathology, including an elastofibroma dorsi (#003) and two areas of fibrosis/scarring in breast tissue (#011), respectively.

*Cancer tissues:* The average  $^{68}\text{Ga}$ -FAPi-46 SUVmean and SUVmax was  $7.2 \pm 4.4$  (range 1.5-15.2) and  $8.6 \pm 5.2$  (range 1.7-19) in primary tumors (N=15) and  $4.3 \pm 2.9$  (range 2.1-8.8) and  $5.3 \pm 3.6$  (range 2.7-10.8) in metastases (N=6), respectively. The cancer types with highest  $^{68}\text{Ga}$ -FAPi-46 uptake were those from pancreas, stomach, colon and uterus. The lowest uptake was observed in two patients with complete response to neoadjuvant therapy (#013 and #015) and thus low FAP expression

### **Immunohistochemistry Findings**

Histologic sections from surgical pathology cases of 13 patients who underwent tumor resection were analyzed. Normal tissue adjacent to tumors and tumor tissue from individual histological sections were available for immunohistochemistry in 13/15 (87%) and 11/15 patients (73%), respectively. Primary tumor, metastasis, or both primary tumor

and metastasis were evaluated in 7/11 (63%), 2/11 (18%), 2/11 (18%) cases, respectively. The FAP scoring between the 2 pathologists was in almost perfect agreement (K=0.89).

*Primary Tumors:* The highest FAP immunohistochemistry scores were observed in pancreatic, esophageal and breast cancer. FAP staining was exclusively confined to the tumor-associated stromal compartment in most patients (12/13; 92.3%) and ranged from weak to strong expression (1-3). Staining intensity was greatest in stromal areas within and immediately adjacent (peritumoral) to the malignant epithelial compartment of tumors as shown in a case example in Figure 2 (patient #010).

*Metastatic lesions:* All four evaluated metastatic lesions (3 LNs and one liver metastasis) were positive for FAP, including stromal staining in 3/4 and malignant epithelial cell staining in 1/4 (uterine squamous cell carcinoma involving a left pelvic LN, #008). Of note, FAP staining was equivalent between primary and metastatic lesions in 2 patients with tissue available for comparative analysis (#006 and #015, Supplemental Figure 2).

*Non-cancer tissues:* Staining was absent or weak in the majority of normal tissues (71.4% negative, 25% weak, 3.6% moderate) and primarily observed in capillary and small vessel endothelium FAP expression was moderate in a concurrently resected benign elastofibroma dorsi (#003), as well as moderate to strong in two areas radial scar and biopsy site changes in benign breast tissue without cancer (#011, Supplemental Figure 3).

### **Correlation of the <sup>68</sup>Ga-FAPi-46 PET Signal and FAP Immunohistochemistry Staining in cancer and non-cancer tissues (Per-Patient Analysis)**

Supplemental Figures 4-16 depict each patient case with available cross-sectional correlation analysis of the <sup>68</sup>Ga-FAPi-46 PET Signal and FAP immunohistochemistry staining score.

<sup>68</sup>Ga-FAPi-46 SUVmax, SUVmean and FAP immunohistochemistry score were higher in cancer tissue than in normal tissue: mean SUVmax 7.7 (95% CI 5.1-10.3) versus 1.6 (95% CI 0.9-2.2, p<0.001, mean SUVmean 6.2 (95% CI 4.0-8.3) versus 1.0 (95% CI

0.7-1.3,  $p < 0.001$ ) and mean FAP immunohistochemistry score 2.8 (95% CI, 2.6-3.0,  $p < 0.001$ ) versus 0.9 (95% CI, 0.4-1.4,  $p < 0.001$ ), respectively (Figure 3).

The FAP immunohistochemistry score was positively correlated with both  $^{68}\text{Ga}$ -FAPi-46 SUVmax across cancer and non-cancer issues ( $r = 0.781$  (95% CI 0.376-0.936),  $p < 0.001$ ) and SUVmean ( $r = 0.783$  (95% CI 0.379-0.936),  $p < 0.001$ ) (Figure 4). FAP immunohistochemistry score 0, score 1, score 2 and score 3 corresponded to a mean  $^{68}\text{Ga}$ -FAPi-46 SUVmax of 1.2 (95%CI 0.8-1.6), 1.9 (95%CI 0.4-3.3), 3.9 (95%CI 2.8-4.9) and 7.4 (95%CI 4.5-10.3), respectively. CT size tended to be positively correlated with SUVmax (Spearman correlation  $r = 0.57$ ;  $p = 0.054$ ) and SUVmean (Spearman correlation  $r = 0.54$ ;  $p = 0.068$ ).

## DISCUSSION

In this translational study we aimed to establish the spectrum of FAP expression across various cancers by immunohistochemistry and to explore whether  $^{68}\text{Ga}$ -FAPi-46 PET biodistribution faithfully reflects FAP expression in cancer patients. We report here the results of a tissue microarray analysis from 141 patients with 14 different types of cancer and of an interim analysis of a prospective exploratory imaging trial that included 15 patients. FAP was expressed across all cancer types with variable intensity and frequency. We established a positive and significant correlation between FAP-target expression and FAPi PET SUVs.

Cancer-associated fibroblasts are key constituents of the tumor stroma that can support an immunosuppressive microenvironment, tumor cell growth, progression and metastatic potential (1). Depleting the stroma can improve delivery of drugs or systemically applied radiation and enhance cancer immune responses (15). Thus, fibroblast activation protein expressed by cancer-associated fibroblasts is an attractive diagnostic and therapeutic target (16). Target specificity and tumor-specific uptake are critical determinants of the accuracy and efficacy of PET probes for diagnosis and therapy (17). FAP is frequently highly expressed in solid tumors with only limited expression in normal tissues, making it an attractive theranostic target (10).

FAPi PET imaging has reported high tumor-to-background characteristics (10). However, FAPi PET human biodistribution in cancer has not been validated against tumor

FAP expression as assessed by immunohistochemistry in a pan-cancer approach. Recently, a study showed a strong association of tumor  $^{68}\text{Ga}$ -FAPi-46 PET uptake intensity and histopathological FAP expression in sarcoma tumors (18). Here, we first screened TMAs from 14 cancers for FAP expression to guide patient selection for the exploratory imaging trial. Guided by our initial TMA screening, we intentionally selected multiple cancer types to validate the pan-cancer approach. In the interim analysis of this prospective exploratory trial the biodistribution of  $^{68}\text{Ga}$ -FAPi-46 PET strongly correlated with FAP expression in cancer versus normal tissues across 7 different cancer types, supporting its potential role as pan-cancer predictive biomarker for FAP-targeted therapies. In a subset of patients,  $^{68}\text{Ga}$ -FAPi-46 SUVmax of metastasis were also comparable to their primary tumor suggesting FAP expression may be consistent across primary and metastatic lesions within individual patients, which has important implications for its role as a theranostic in the setting of advanced disease (19).

These findings support further exploration of  $^{68}\text{Ga}$ -FAPi-46 as a potential pan-cancer imaging biomarker for FAP expression. This could find application as an enrichment biomarker or patient selection tool for clinical trials and as potential predictors of treatment response in the clinic. Extensive emerging data implicate FAP-positive cells as important accomplices involved in cancer progression and metastases. Evaluating FAP-targeting small molecule inhibitors, antibodies, bispecific T-cell engagers and radioligand therapy requires means for verifying whole-body target expression (20).

### ***Limitations***

The main limitation of the study was the small sample size. This was an exploratory study and local oversight committees (ISPRC, DSMB) mandated an interim analysis after the first 15 patients. This interim analysis revealed a highly 14 significant correlation between immunohistochemistry and PET findings, which provided the motivation to publish the data.

Another major limitation is the intra-tumor heterogeneity and sampling bias inherent to the histopathology and immunochemistry analysis. Unfortunately, autoradiography was not possible in this exploratory study because a second administration of  $^{68}\text{Ga}$ -FAPi-46 just before surgery was not practical. We performed an evaluation of all H&E slides from each surgical pathology case to select one

representative section best representing the overall tumor histology and/or its surrounding adjacent normal tissue.

A perfect anatomical match between tumor SUV measurements and immunohistochemistry scores was unfortunately not possible because tumors were not resected in a defined orientation (unlike in prostate cancer). Therefore, we collected the SUVmax and SUVmean of the whole tumor lesion.

Another limitation is that visual immunohistochemistry scoring by pathologist is semi-quantitative only, subjective and produces ordinal rather than continuous variable data. Computer-aided analysis with automatic immunohistochemistry scoring may overcome these limitations. However even with semi-quantitative ordinal data, the correlation of immunohistochemistry score with SUV was very strong. Furthermore, the inter-reader scores between the 2 pathologists was in near perfect agreement.

## **CONCLUSION**

In this interim analysis of a prospective exploratory imaging trial,  $^{68}\text{Ga}$ -FAPi-46 PET biodistribution correlated strongly with FAP expression in cancer and non-cancer tissues across multiple cancer types. These data support the use of  $^{68}\text{Ga}$ -FAPi-46 PET as a pan-cancer predictive biomarker and stratification tool for FAP-targeted therapeutic approaches and lay the foundation for future evaluation of FAPi ligand labeled with therapeutic isotopes in clinical trials.

## **FUNDING**

This was an investigator-initiated trial with support from the Society of Nuclear Medicine and Molecular Imaging (SNMMI, 2019 Molecular Imaging Research Grant for Junior Academic Faculty #20194491 (PI:JCa)), and the Prostate Cancer Foundation (PCF, 2019 Challenge Award 19CHAL02(PI:JCz), 2020 Young Investigator Award 20YOUN05 (PI:JCa)).

## **DECLARATION OF CONFLICTS OF INTEREST**

Johannes Czernin is a founder, holds equity and is a board member of Sofie Biosciences and Momentum Biosciences that have licensed intellectual property of FAPi compounds from the University of Heidelberg. He is also a cofounder of Trethera Therapeutics and serves on the Medical Advisory Boards of Point Pharma and Actinium Pharmaceuticals. Jeremie Calais reports prior consulting activities for Advanced Accelerator Applications, Blue Earth Diagnostics, Curium Pharma, GE Healthcare, Janssen Pharmaceuticals, Progenics Radiopharmaceuticals, Radiomedix and Telix Pharmaceuticals, outside of the submitted work.

Christine Mona and Katharina Lueckerath report consulting activities for Sofie Biosciences /iTheranostics outside of the submitted work.

No other potential conflicts of interest relevant to this article exist.

## **ACKNOWLEDGMENTS**

We thank all the patients and their referring physicians whose willingness to participate made this study possible. We thank the whole staff of the University of California Los Angeles (UCLA; Los Angeles, CA, USA) Nuclear Medicine and Theranostics Division whose hard work made this study possible. The authors would like to thank the UCLA Translational Pathology Core Laboratory for their excellent technical assistance.

## **KEY POINTS**

**Question:** Is FAPi PET imaging a reliable biomarker of FAP expression in cancer and non-cancer tissues?

**Pertinent findings:** In this translational study using tissue microarrays and an interim analysis of a prospective exploratory imaging trial in 15 surgical oncology patients, the FAPi PET uptake and FAP expression per immunohistochemistry were strongly correlated in cancer and non-cancer tissue.

**Implications for patient care:** FAPi PET uptake correlates strongly with FAP expression in cancer patients and FAPi PET may thus serve as predictive biomarker for FAP-targeted therapeutic approaches.

## REFERENCES

1. Gascard P, Tlsty TD. Carcinoma-associated fibroblasts: orchestrating the composition of malignancy. *Genes Dev.* 2016;30:1002-1019.
2. Fitzgerald AA, Weiner LM. The role of fibroblast activation protein in health and malignancy. *Cancer Metastasis Rev.* 2020;39:783-803.
3. Lo A, Wang LS, Scholler J, et al. Tumor-Promoting Desmoplasia Is Disrupted by Depleting FAP-Expressing Stromal Cells. *Cancer Res.* 2015;75:2800-2810.
4. Fearon DT. The carcinoma-associated fibroblast expressing fibroblast activation protein and escape from immune surveillance. *Cancer Immunol Res.* 2014;2:187-193.
5. Kraman M, Bambrough PJ, Arnold JN, et al. Suppression of antitumor immunity by stromal cells expressing fibroblast activation protein- $\alpha$ . *Science.* 2010;330:827-830.
6. Eager RM, Cunningham CC, Senzer N, et al. Phase II trial of talabostat and docetaxel in advanced non-small cell lung cancer. *Clin Oncol (R Coll Radiol).* 2009;21:464-472.
7. Liu R, Li H, Liu L, Yu J, Ren X. Fibroblast activation protein: A potential therapeutic target in cancer. *Cancer Biol Ther.* 2012;13:123-129.
8. Loktev A, Lindner T, Burger EM, et al. Development of Fibroblast Activation Protein-Targeted Radiotracers with Improved Tumor Retention. *J Nucl Med.* 2019;60:1421-1429.
9. Loktev A, Lindner T, Mier W, et al. A Tumor-Imaging Method Targeting Cancer-Associated Fibroblasts. *J Nucl Med.* 2018;59:1423-1429.

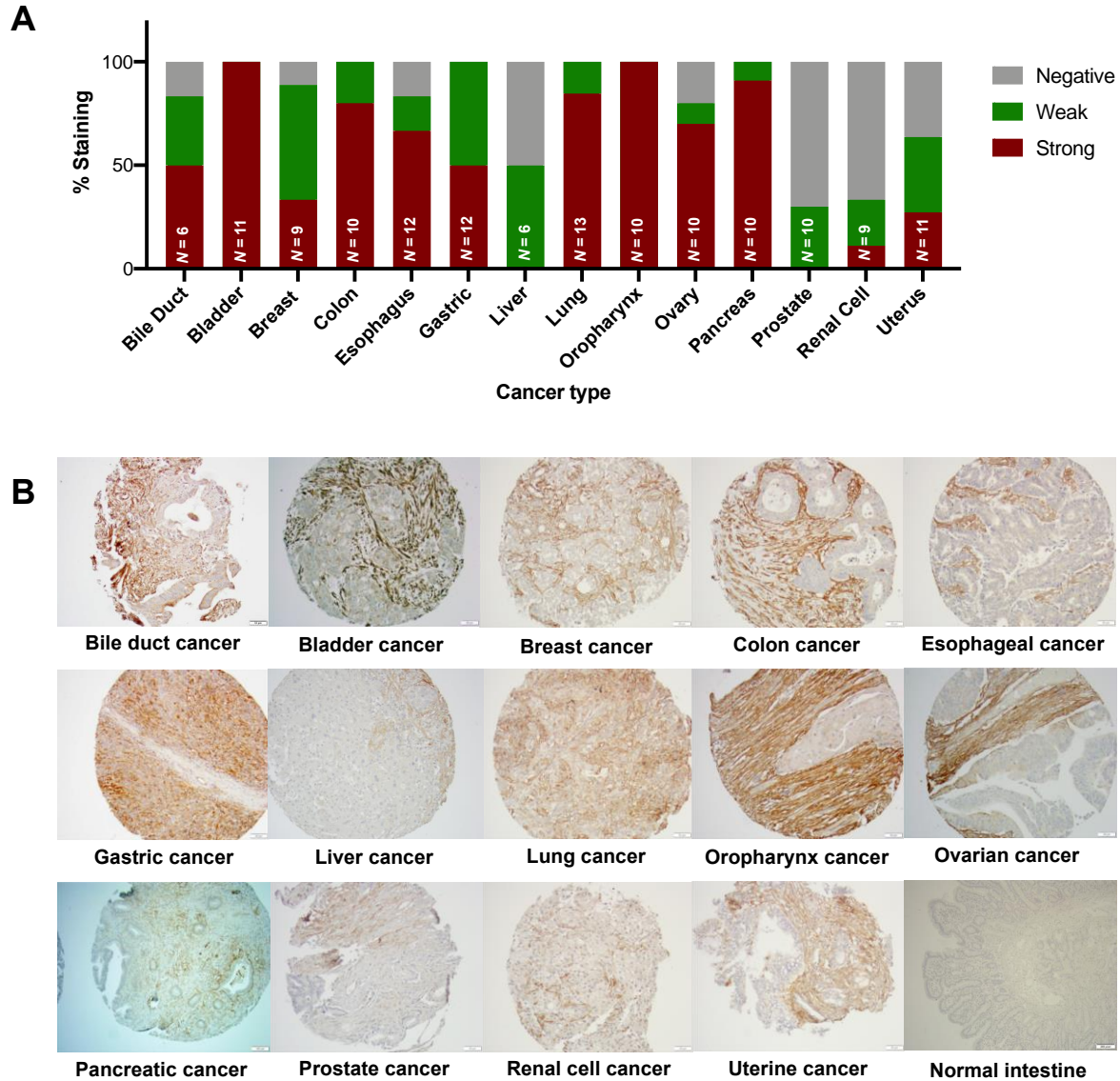


10. Kratochwil C, Flechsig P, Lindner T, et al. (68)Ga-FAPI PET/CT: Tracer Uptake in 28 Different Kinds of Cancer. *J Nucl Med.* 2019;60:801-805.
11. Kallioniemi OP, Wagner U, Kononen J, Sauter G. Tissue microarray technology for high-throughput molecular profiling of cancer. *Hum Mol Genet.* 2001;10:657-662.
12. Rosset A, Spadola L, Ratib O. OsiriX: an open-source software for navigating in multidimensional DICOM images. *J Digit Imaging.* 2004;17:205-216.
13. Henry LR, Lee HO, Lee JS, et al. Clinical implications of fibroblast activation protein in patients with colon cancer. *Clin Cancer Res.* 2007;13:1736-1741.
14. Bakdash JZ, Marusich LR. Repeated Measures Correlation. *Front Psychol.* 2017;8:456.
15. Barsoumian HB, Ramapriyan R, Younes AI, et al. Low-dose radiation treatment enhances systemic antitumor immune responses by overcoming the inhibitory stroma. *J Immunother Cancer.* 2020;8:e000537.
16. Narunsky L, Oren R, Bochner F, Neeman M. Imaging aspects of the tumor stroma with therapeutic implications. *Pharmacol Ther.* 2014;141:192-208.
17. Huang R, Wang M, Zhu Y, Conti PS, Chen K. Development of PET probes for cancer imaging. *Curr Top Med Chem.* 2015;15:795-819.
18. Kessler L, Ferdinandus J, Hirnas N, et al. Ga-68-FAPI as diagnostic tool in sarcoma: Data from the FAPI-PET prospective observational trial. *J Nucl Med.* 2021:ePub.
19. Arranja AG, Pathak V, Lammers T, Shi Y. Tumor-targeted nanomedicines for cancer theranostics. *Pharmacol Res.* 2017;115:87-95.

20. Lindner T, Loktev A, Giesel F, Kratochwil C, Altmann A, Haberkorn U. Targeting of activated fibroblasts for imaging and therapy. *EJNMMI Radiopharm Chem.* 2019;4:16.
21. Targeted Alpha Therapy Working G, Parker C, Lewington V, et al. Targeted Alpha Therapy, an Emerging Class of Cancer Agents: A Review. *JAMA Oncol.* 2018;4:1765-1772.
22. Asadian S, Mirzaei H, Kalantari BA, et al. beta-radiating radionuclides in cancer treatment, novel insight into promising approach. *Pharmacol Res.* 2020;160:105070.

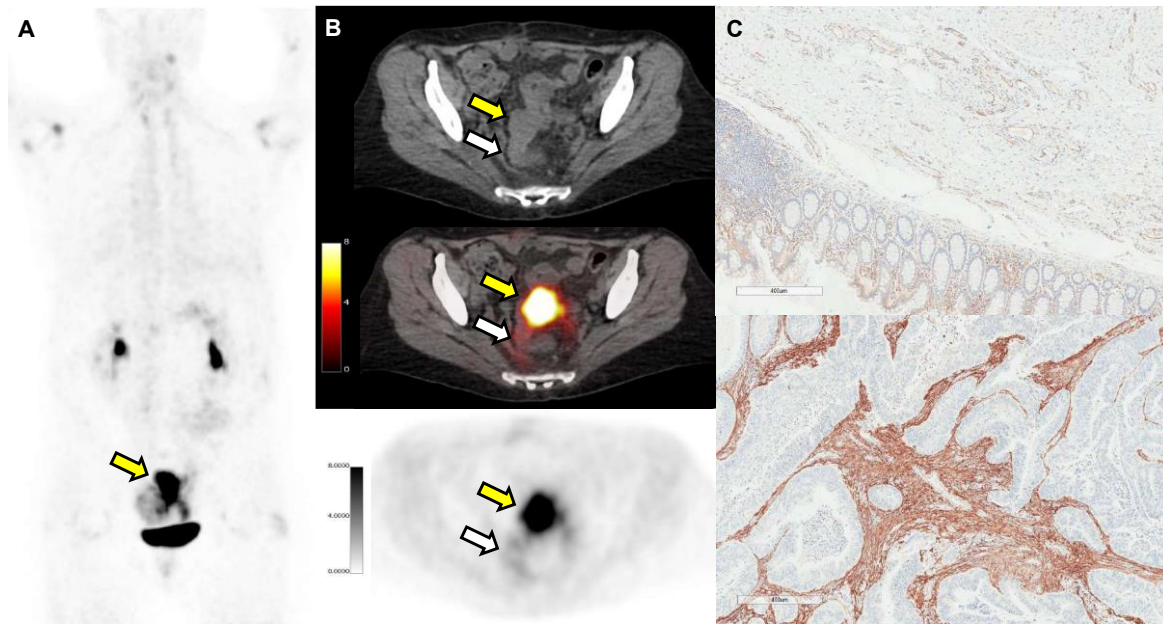
## FIGURES

**Figure 1: FAP expression by immunohistochemistry in 14 cancer types and normal tissues (tissue microarrays analysis)**



(A) Quantification of FAP expression per cancer type. FAP intensity was evaluated using a semi-quantitative scoring system that accounts for staining intensity (0–2: 30 = negative, 1 = weak, 2 = strong). (B) FAP immunohistochemistry expression on representative tissue core from indicated cancer or normal tissue type.

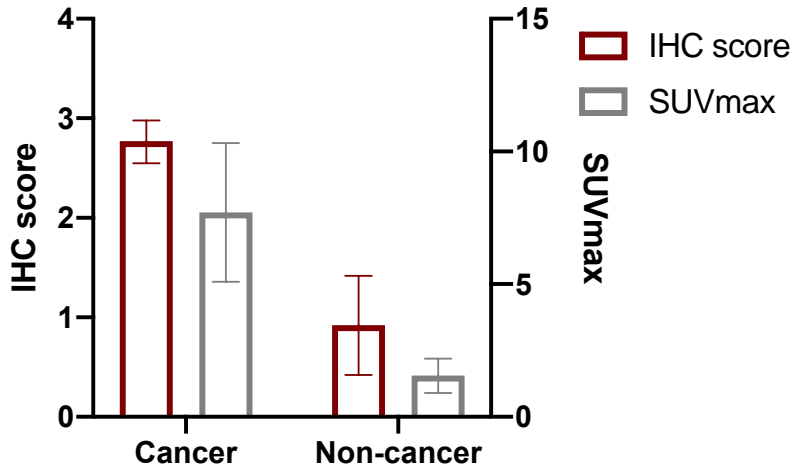
**Figure 2: Matched  $^{68}\text{Ga}$ -FAPi-46 PET/CT and immunohistochemistry of patient #010**



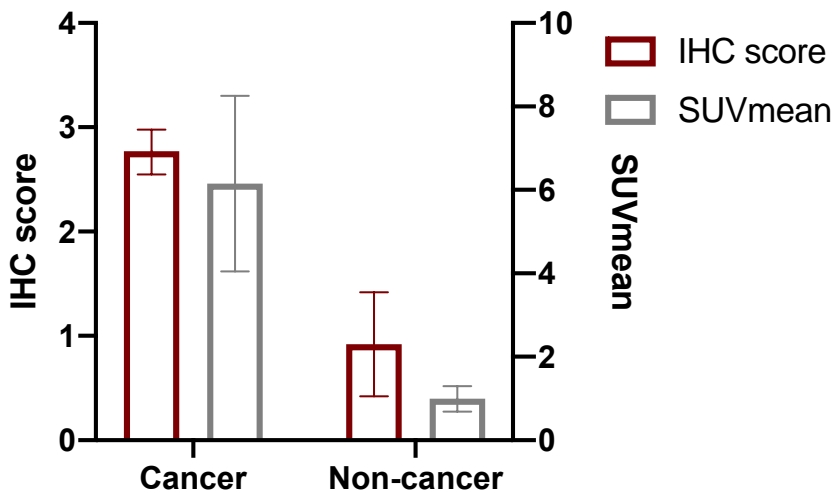
56-year-old female patient with sigmoid colon adenocarcinoma who underwent colorectal anterior resection (ypT4b N0 M0). In correspondence of the resected mass as shown by the yellow arrows ((A): PET Maximum Intensity Projection (MIP), (B) axial CT, (C) axial fusion PET/CT, (D) axial PET),  $^{68}\text{Ga}$ -FAPi-46 PET/CT showed intense uptake (SUVmax 15.9 and SUVmean 12.8). FAP immunohistochemistry on representative histologic sections demonstrated absent to weak FAP expression seen predominantly as vessel endothelial cell staining in normal (C top panel) and strong FAP expression in intratumoral and peritumoral stromal (C lower panel). White arrows depict normal region resected.

**Figure 3:  $^{68}\text{Ga}$ -FAPi-46 FAPi PET SUVs and FAP immunohistochemistry score in non-cancer and cancer tissue**

**A**

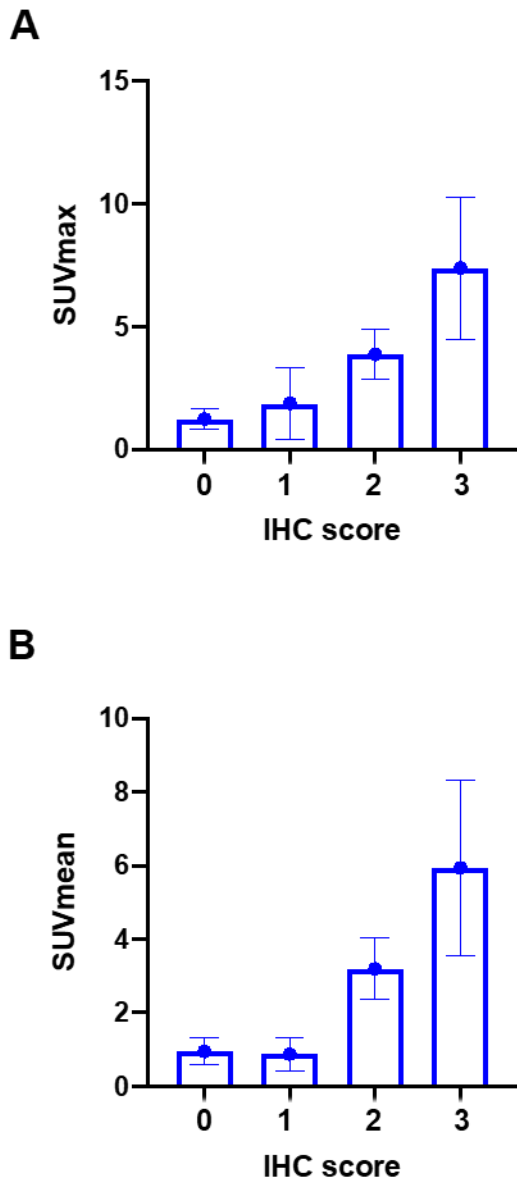


**B**



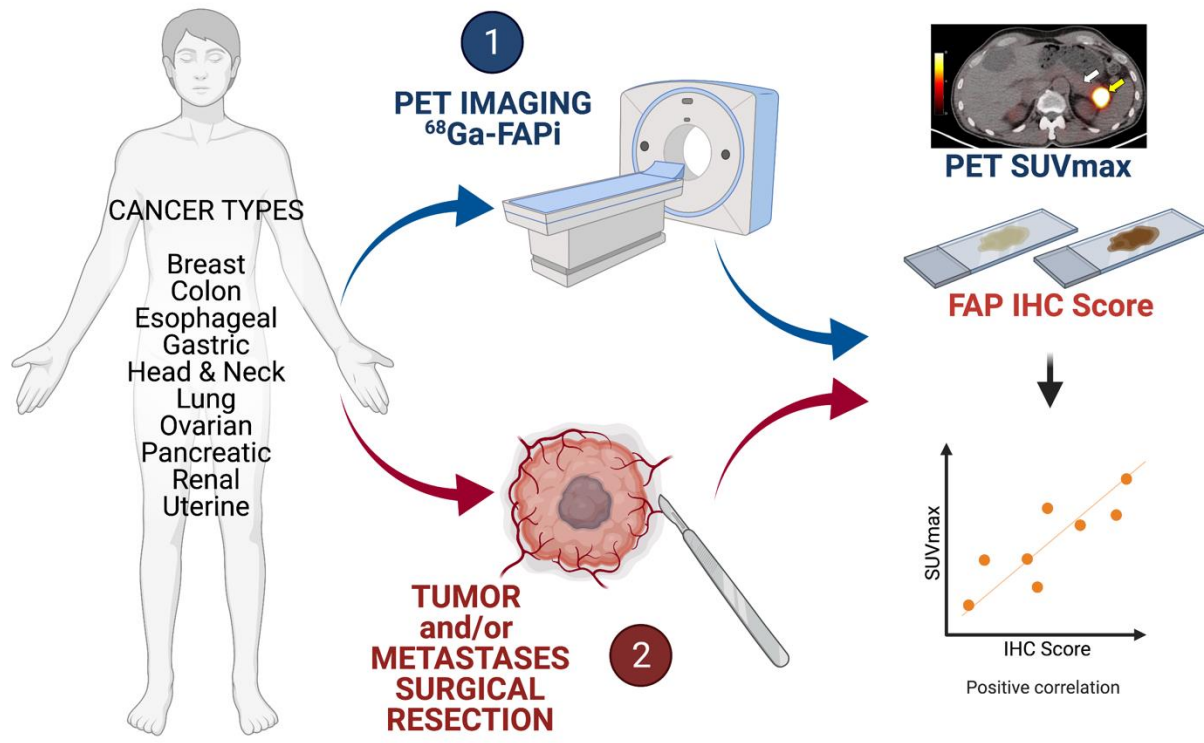
FAP immunohistochemistry score with  $^{68}\text{Ga}$ -FAPi-46 PET SUVmax (A) and SUVmean (B) in cancer and non-cancer tissue. Each bar represents the mean with standard deviation.

**Figure 4: Correlation between FAP immunohistochemistry score and <sup>68</sup>Ga-FAPi-46 PET SUVs across cancer and non-cancer issues**



<sup>68</sup>Ga-FAPi-46 SUVmax (A), SUVmean (B) and FAP immunohistochemistry score with positive correlation  $r=0.781$  (95% CI 0.376-0.936),  $p<0.001$ ),  $r=0.783$  (95% CI 0.379-0.936),  $p<0.001$ ).

# Graphical Abstract



**Supplemental Table 1: Inclusion and exclusion criteria of the clinical trial NCT04147494**

---

***Inclusion criteria***

---

Patients with the following cancer types:

- Breast cancer
- Colon cancer
- Esophageal cancer
- Gastric cancer
- Head and Neck cancer
- Lung cancer
- Ovarian cancer
- Pancreatic cancer
- Renal cancer
- Uterus Cancer

Patients who are scheduled to undergo surgical resection of the primary tumor and/or metastasis.

Patients are  $\geq 18$  years old at the time of the radiotracer administration.

Patient can provide written informed consent.

Patient is capable of complying with study procedures.

Patient is able to remain still for duration of imaging procedure (up to one hour).

---

***Exclusion criteria***

---

Patient is pregnant or nursing.

Patient has underlying disease which, based on the judgment of the investigator, might interfere with the collection of high-quality data.

---



**Supplemental Table 2: Study population demographics and clinical characteristics**

Patient ID#	Age	Gender	Race	Cancer type	Organ	Histologic type	Surgical Procedure	pTNM
#001	51	M	Hispanic	Head and Neck	Oral mucosa left mandible	Squamous cell carcinoma	Left Composite Mandibulectomy With Left Neck Dissection	pT4a N0 M0
#002	71	M	Caucasian	Esophageal	Distal and mid esophagus	Squamous cell carcinoma	Esophagogastrectomy	pT1b N0 M0
#003	69	F	Caucasian	Gastric	Gastroesophageal junction	Adenocarcinoma	Not performed	NA
#004	57	M	Caucasian	Head and Neck	Left piriform sinus + cervical lymph nodes	P16+ squamous cell carcinoma	Left partial glossectomy and left neck dissection	pTx N2b M0
#005	76	M	NA	Colon	Cecum	Medullary Carcinoma	Right hemicolectomy	pT2 N0 M0
#006	55	M	African American	Colon	Cecum	Mucinous Adenocarcinoma	Right hemicolectomy	pT3 N1b M0
#007	68	F	African American	Head and Neck	Right retromolar trigone	Verrucous Squamous Cell Carcinoma	Right mandibulectomy	pT2 N0 M0
#008	36	F	Latino	Uterus	Uterus and lymph nodes	Squamous Cell Carcinoma	Bilateral Salpingectomy + left pelvic lymphadenectomy	pTx N1 M0
#009	65	M	Caucasian	Pancreatic	Pancreas, Tail	Adenocarcinoma	Partial pancreatectomy, pancreatic tail	pT2 N1 M0
#010	56	F	Caucasian	Colon	Sigmoid Colon	Adenocarcinoma	Colo-rectal anterior resection	ypT4b N0 M0
#011	65	F	Caucasian	Breast	Bilateral breasts	Invasive ductal adenocarcinoma	Bilateral Mastectomy	pT1c Nx
#012	61	M	Caucasian	Esophageal	Gastroesophageal junction	Adenocarcinoma	Esophagogastrectomy	pT3 pN2
#013	51	F	other	Breast	Right breast	Invasive ductal carcinoma	Right mastectomy and lymphadenectomy	ypT0 N0 M0
#014	73	M	Caucasian	Pancreatic	Pancreas, head	Adenosquamous carcinoma	Not performed	NA
#015	56	F	Latino	Colon	Left colon + solitary liver metastasis	Adenocarcinoma	Left hemicolectomy	ypT3 N1b M1a

**Supplemental Table 3: <sup>68</sup>Ga-FAPi-46 PET biodistribution in normal organs quantified by SUVmean (n=15 patients)**

<b>Organ</b>	<b><sup>68</sup>Ga-FAPi-46 uptake SUVmean Average ±SD (range)</b>
1. Brain	0.03±0.04 (0-0.1)
2. Parotid	1.3±0.3 (0.8-2.0)
3. Submandibular gland	2.5±0.5 (1.5-3.3)
4. Waldeyer's ring	2.0±0.8 (1.1-4.0)
5. Thyroid	1.8±0.6 (1.0-3.5)
6. Blood pool	1.2±0.2 (0.9-1.5)
7. Heart	1.1±0.5 (0.6-2.8)
8. Lung	0.5±0.2 (0.2-1.2)
9. Liver	0.8±0.2 (0.6-1.2)
10. Gallbladder	0.7±0.2 (0.5-1.1)
11. Pancreas	2.0±1.4 (0.6-6.0)
12. Spleen	0.9±0.2 (0.6-1.2)
13. Adrenal	1.0±0.3 (0.4-1.5)
14. Kidney	2.0±0.6 (1.4-3.9)
15. Small bowel	0.8±0.2 (0.5-1.2)
16. Colon	0.8±0.4 (0.3-1.6)
17. Urinary bladder	51.9±28.4 (13.9-108.7)
18. Uterus (n=7)	6.3±3.7 (2.3-13.4)
19. Prostate (n=8)	1.2±0.4 (0.5-1.9)
20. Ovary (n=6)	1.7±0.4 (1.2-2.2)
21. Testis (n=8)	1.6±0.3 (1.2-2.1)
22. Bone marrow	0.7±0.3 (0.4-1.5)
23. Muscle	1.3±0.3 (0.9-2.2)
25. Fat	0.3±0.1 (0.2-0.7)
25. Breast (n=7)	1.4±0.8 (0.7-2.5)

**Supplemental Table 4: <sup>68</sup>Ga-FAPi-46 uptake in primary tumors (n=15 patients)**

Patient	Cancer type	Histologic type	Size (mm)	SUVmax	SUVmean
001	Head/Neck	Carcinoma cuniculatum	13	7.7	6.3
002	Esophagus	Squamous cell carcinoma	13	5.4	4.3
003*	Gastric	Adenocarcinoma	32	7.4	6.0
004	Head/Neck	P16+ squamous cell carcinoma	12	7.4	6.3
005	Colon	Medullary Carcinoma	30	8.1	6.8
006	Colon	Mucinous Adenocarcinoma	16	6.3	5.2
007	Head/Neck	Verrucous Squamous Cell Carcinoma	18	4.7	3.9
008	Uterus	Squamous Cell Carcinoma	38	19.0	15.2
009	Pancreas	Adenocarcinoma	26	15.7	12.5
010*	Colon	Adenocarcinoma	39	15.9	12.8
011	Breast	Invasive ductal adenocarcinoma	10	4.6	4.0
012*	Esophagus	Adenocarcinoma	52	9.1	7.3
013*	Breast	Invasive ductal carcinoma	-	1.7	1.4
014*	Pancreas	Adenosquamous carcinoma	13	13.4	10.6
015*	Colon	Adenocarcinoma	-	2.5	2.0
Average±SD			24±13	8.6±5.2	7.2±4.4

- = no anatomic correlation

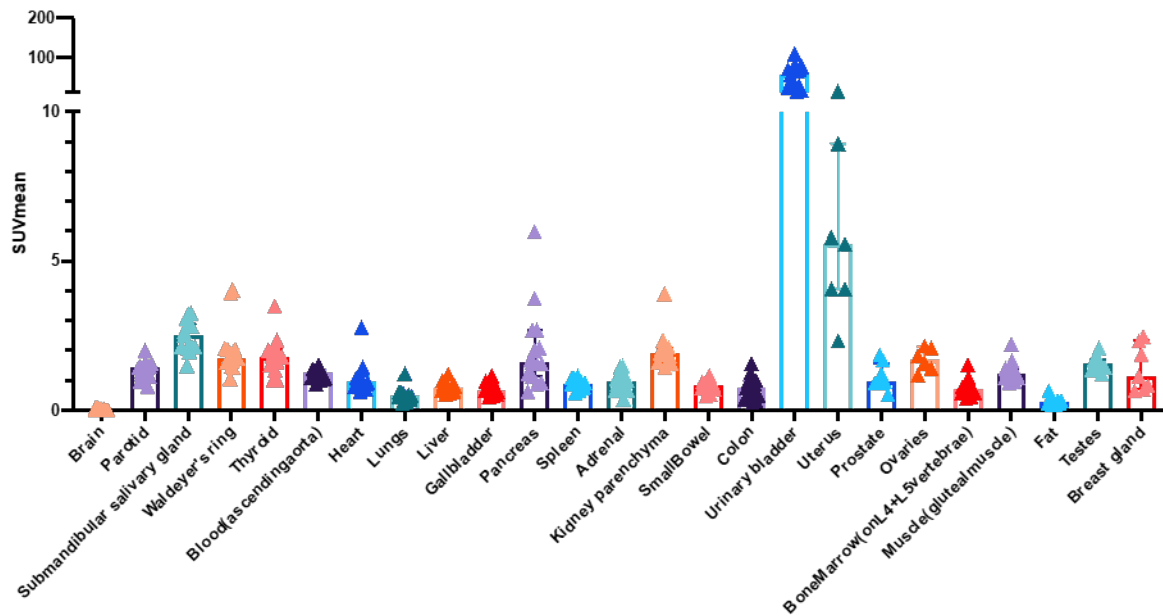
\* = Neo-adjuvant therapy

**Supplemental Table 5: <sup>68</sup>Ga-FAPi-46 uptake in metastases (n= 3 patients)**

Patient	Metastasis Site	Primary Histologic type	Size (mm)	SUVmax	SUVmean
004	Lymph node	SCC (Head/Neck)	20	5.6	4.6
004	Lymph node	SCC (Head/Neck)	20	6.8	5.5
004	Lymph node	SCC (Head/Neck)	19	7.7	6.3
008	Lymph node	SCC (uterus)	21	10.8	8.8
009	Liver	Adenocarcinoma (pancreas)	11	3.5	3.0
015	Liver	Adenocarcinoma (colon)	12	2.7	2.1
Average±SD			17.1±4.1	5.3±3.6	4.3±2.9

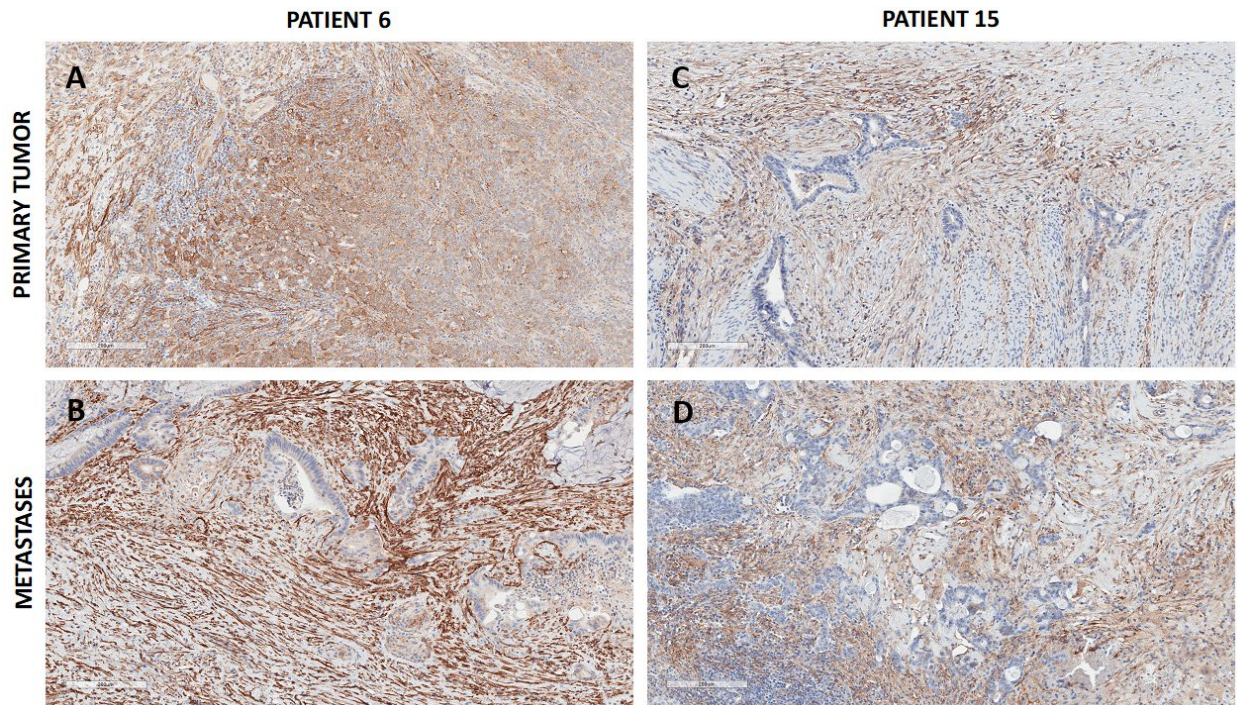
SCC: Squamous Cell Carcinoma

**Supplemental Figure 1:**  $^{68}\text{Ga}$ -FAPi-46 PET biodistribution in normal organs quantified by SUVmean (n=15 patients)



Each bar represents the average SUVmean with standard deviation error bars

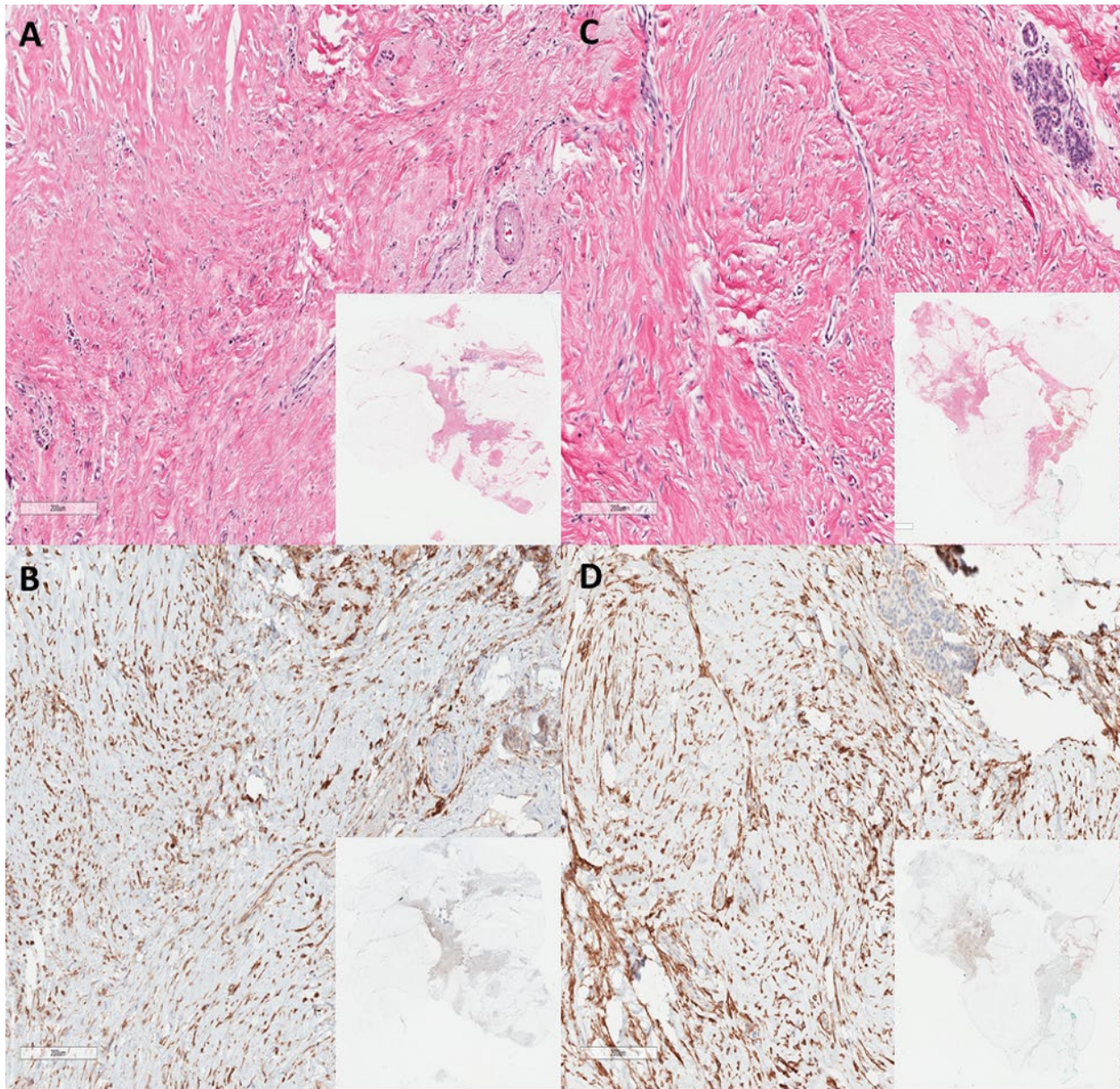
**Supplemental Figure 2. Matched IHC in primary tumor and metastases in patient #006 and #015**



Concordance between IHC score in primary tumor (**A**, top left) and metastatic lesion (**B**, bottom left) from patient #006 showing moderate to strong FAP expression. Concordance between IHC score in primary lesion (**C**, top right) and metastatic lesion (**D**, bottom right) from patient #015 showing moderate FAP expression.

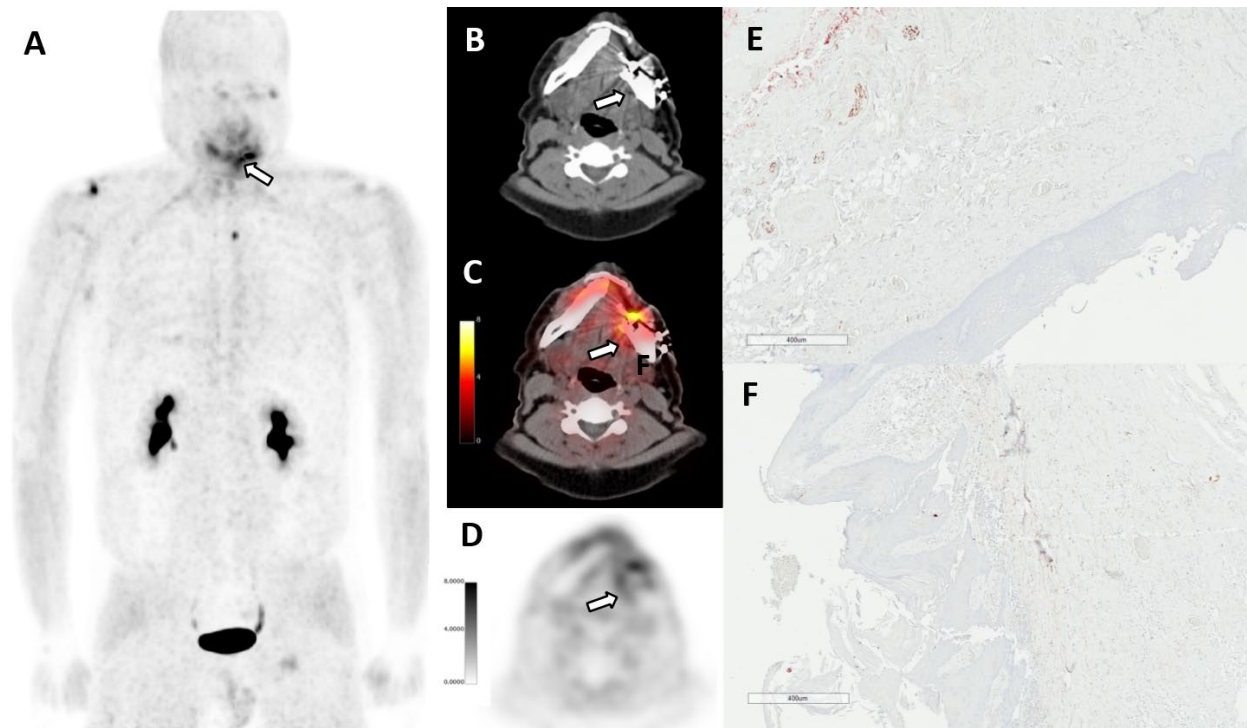


**Supplemental Figure 3: Patient #011 Breast Biopsies immunohistochemistry**



A 65-year-old female patient with 65-year-old female patient with bilateral breast invasive ductal adenocarcinoma. H&E and FAP IHC of histologic sections of left (**A** and **B**) and right (**C** and **D**) demonstrated weak to moderate FAP expression in radial scar tissues.

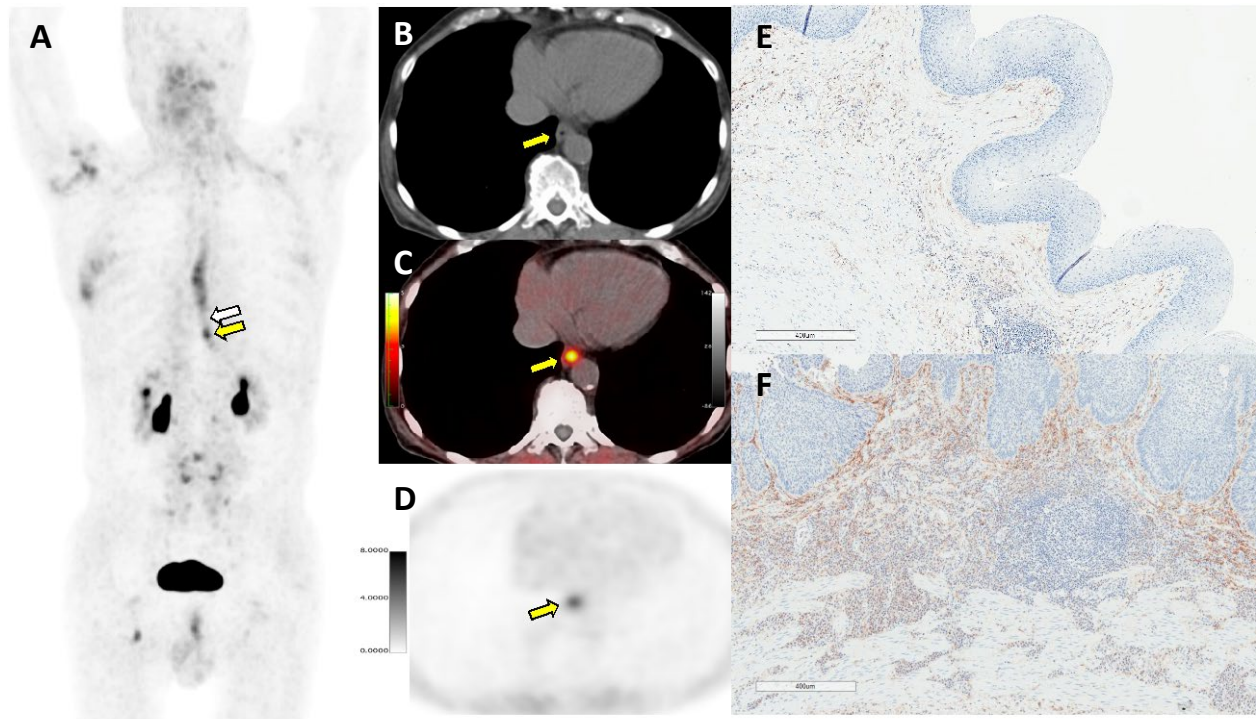
**Supplemental Figure 4: Patient #001 matched  $^{68}\text{Ga}$ -FAPi-46 PET/CT and immunohistochemistry**



51-year-old male patient with squamous cell carcinoma (carcinoma cuniculatum) of the oral mucosa who underwent left composite mandibulectomy with left neck dissection (pT4a N0 M0). In correspondence of the resected lesion as shown by the white arrows,  $^{68}\text{Ga}$ -FAPi-46 PET/CT showed moderate diffuse increased signal (**A**: Maximum Intensity Projection (MIP), **B**: transaxial CT, **C** and **D**: transaxial PET/CT and PET, SUVmax 7.7 and SUVmean 6.3, respectively). FAP IHC on representative histologic sections of normal (**E**) and tumor (**F**) tissue demonstrated absent FAP expression in both, indicative of either a histologic sampling bias or PET overcorrection artefact from dense material.

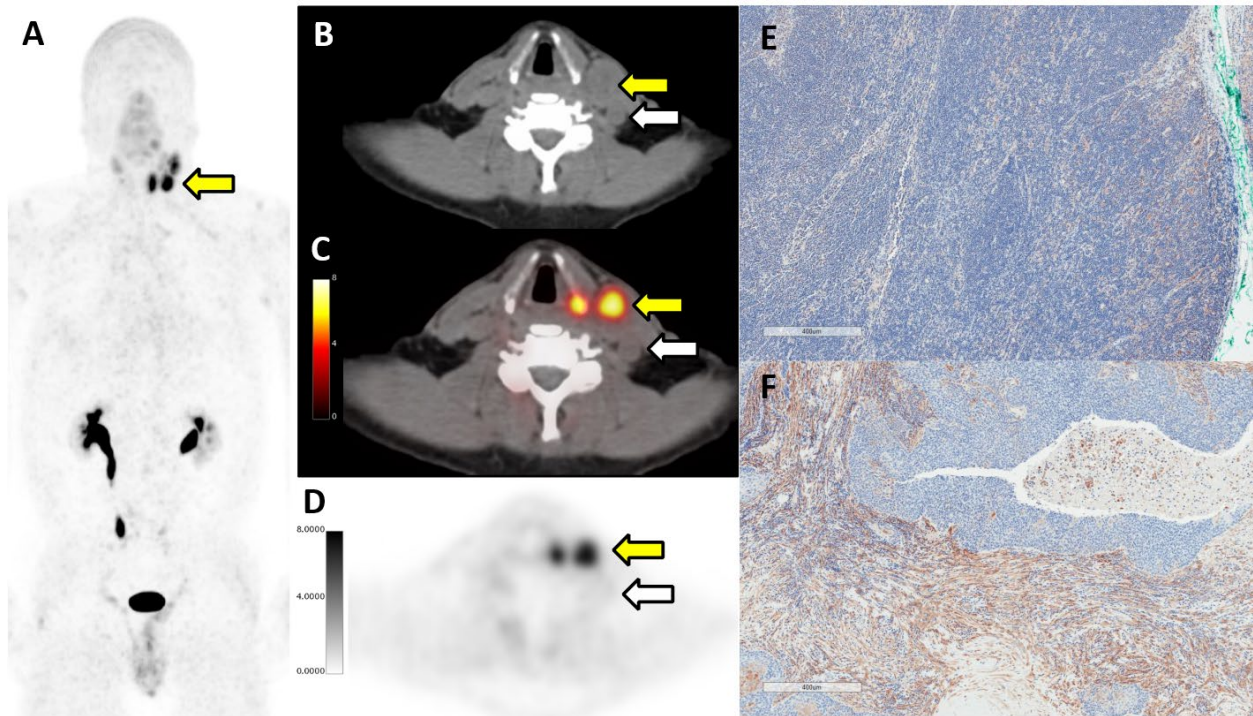


**Supplemental Figure 5: Patient #002 matched  $^{68}\text{Ga}$ -FAPi-46 PET/CT and immunohistochemistry**



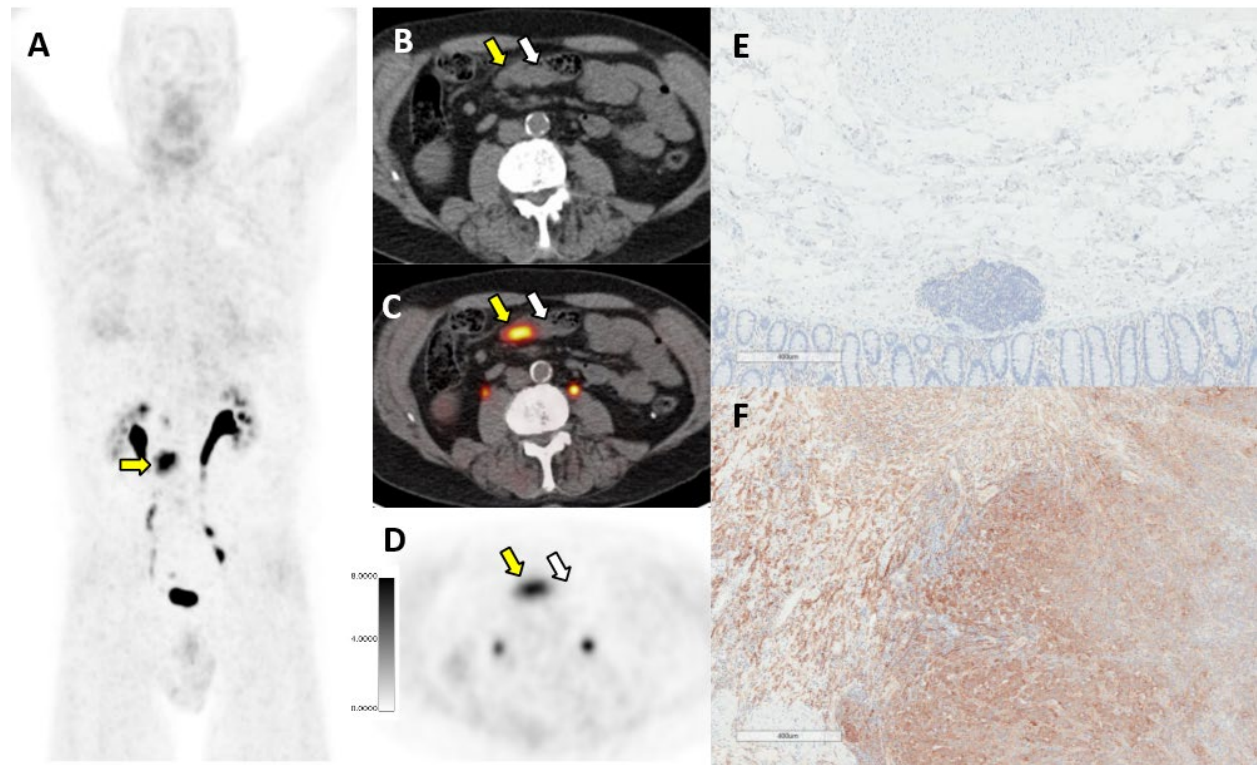
71-year-old male patient with esophageal adenocarcinoma who underwent esophagogastrectomy (pT1b N0 M0). In correspondence of the resected lesion as shown by the yellow arrows,  $^{68}\text{Ga}$ -FAPi-46 PET/CT showed moderate focal uptake (**A**: Maximum Intensity Projection (MIP), **B**: transaxial CT, **C** and **D**: transaxial PET/CT and PET, SUVmax 5.4 and SUVmean 4.3, respectively). FAP IHC on representative histologic sections demonstrated absent to patchy and weak FAP expression for normal tissue (**E**) and weak to moderate FAP expression for tumor tissue (**F**). White arrow depicts resected non-cancer esophagus region.

**Supplemental Figure 6: Patient #004 matched  $^{68}\text{Ga}$ -FAPi-46 PET/CT and immunohistochemistry**



57-year-old male patient with head-and-neck squamous cell carcinoma cancer who underwent left partial glossectomy and left neck dissection (pTx N2b M0). In correspondence of the resected enlarged neck lymph nodes as shown by the yellow arrows  $^{68}\text{Ga}$ -FAPi-46 PET/CT showed intense uptake (**A**: Maximum Intensity Projection (MIP), **B**: transaxial CT, **C** and **D**: transaxial PET/CT and CT, SUVmax 7.4 and SUVmean 6.3, respectively). FAP IHC on representative histologic sections demonstrated no FAP expression in normal tissue (**E**) and moderate to strong FAP expression in tumor tissue (**F**). White arrows depict resected normal lymph node.

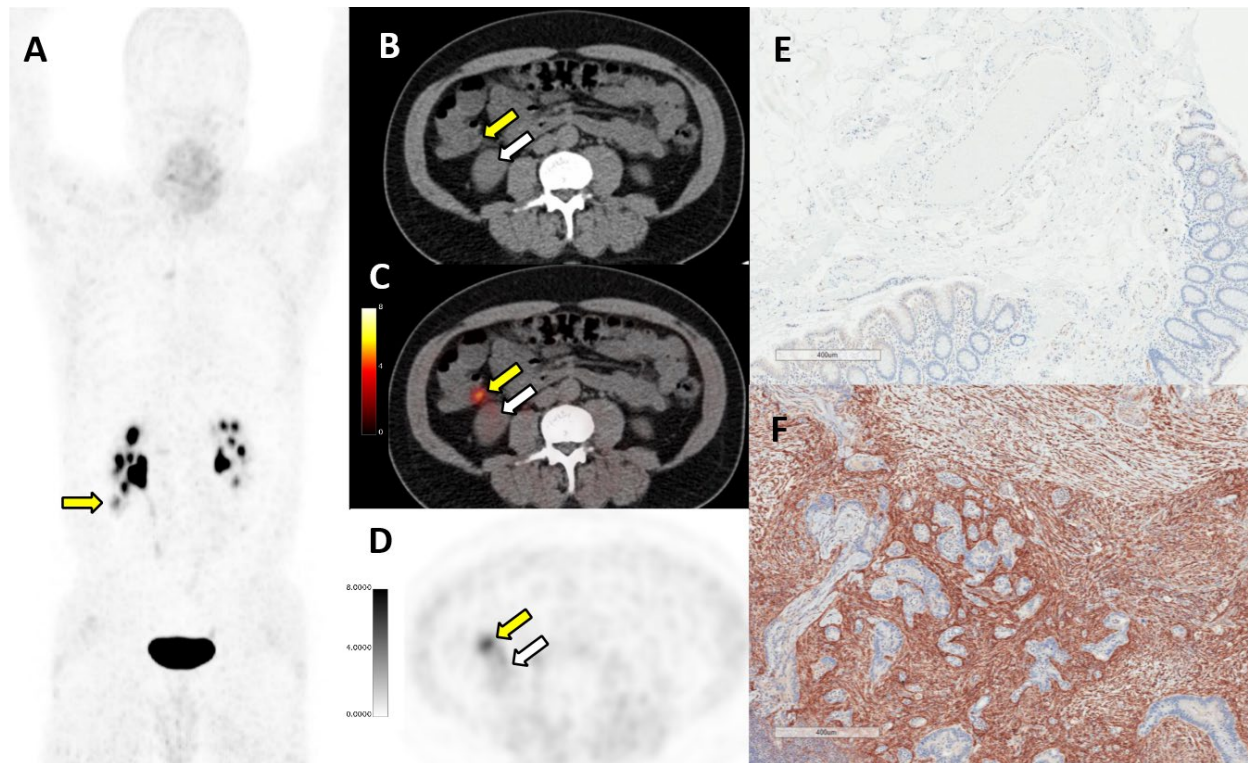
**Supplemental Figure 7: Patient #005 matched  $^{68}\text{Ga}$ -FAPi-46 PET/CT and immunohistochemistry**



57-year-old male patient with medullary adenocarcinoma of the cecum who underwent right hemicolectomy (pT2 N0 M0). In correspondence of the resected lesion as shown by the yellow arrows  $^{68}\text{Ga}$ -FAPi-46 PET/CT showed intense uptake (**A**: Maximum Intensity Projection (MIP), **B**: transaxial CT, **C** and **D**: transaxial PET/CT and CT, SUVmax 8.1 and SUVmean 6.8, respectively). FAP IHC on representative histologic sections demonstrated no FAP expression in normal tissue (**E**) and moderate to strong FAP expression in tumor tissue (**F**). White arrows depict resected normal colon region.

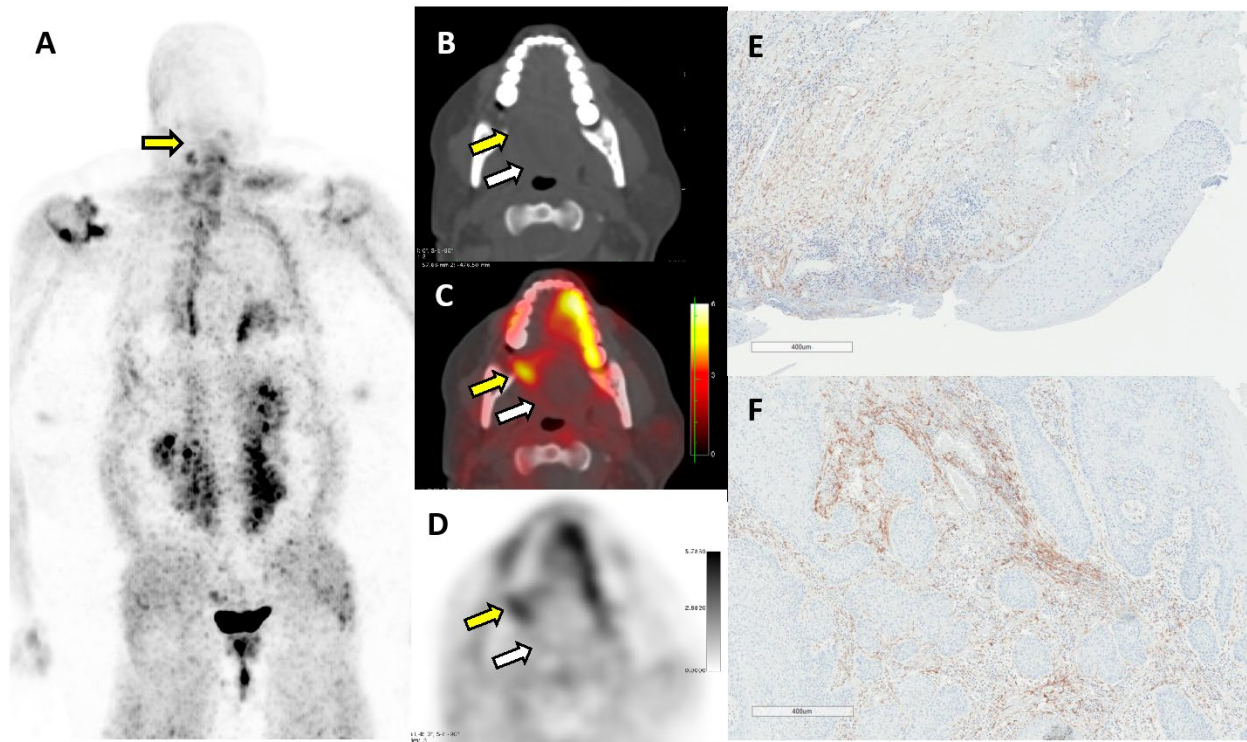


**Supplemental Figure 8: Patient #006 matched  $^{68}\text{Ga}$ -FAPi-46 PET/CT and immunohistochemistry**



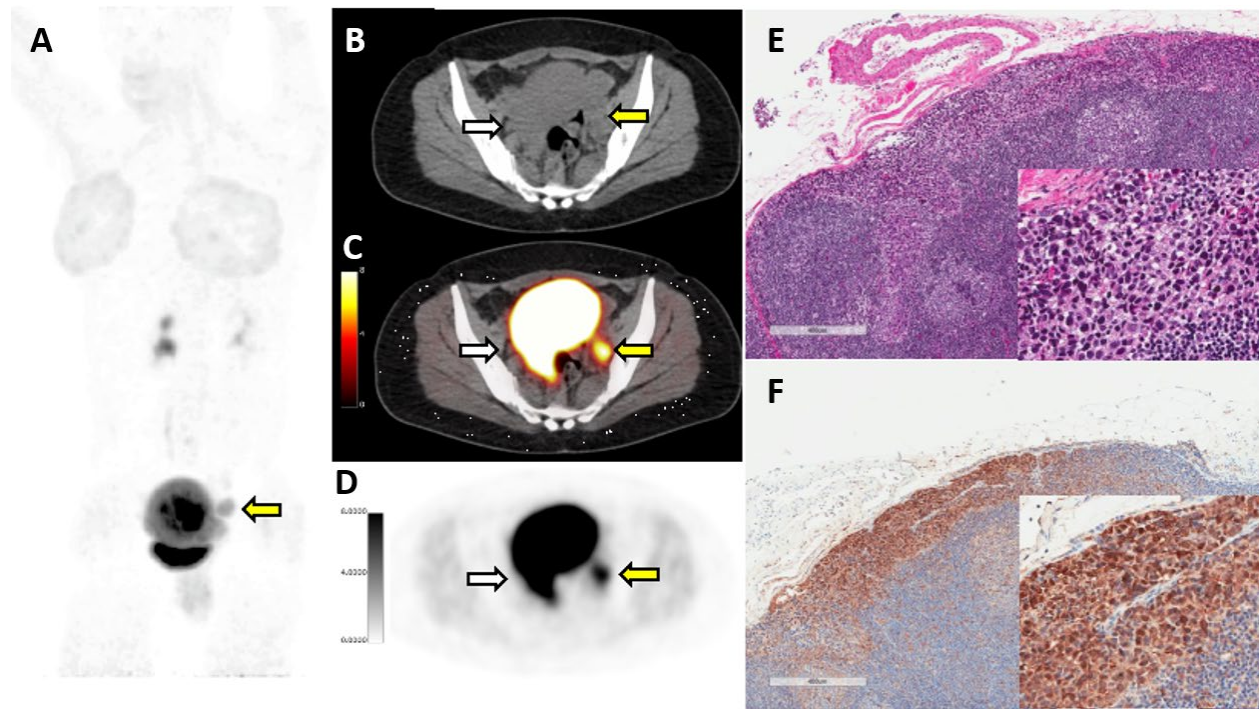
55-year-old male patient with mucinous adenocarcinoma of the cecum who underwent right hemicolectomy (pT3 N1b M0). In correspondence of the resected lesion as shown by the yellow arrows,  $^{68}\text{Ga}$ -FAPi-46 PET/CT showed increased focal uptake (**A**: Maximum Intensity Projection images (MIP), **B**: transaxial CT, **C** and **D**: transaxial PET/CT and PET, SUVmax 6.3 and SUVmean 5.2, respectively). FAP IHC on representative histologic sections demonstrated no FAP expression in normal tissue (**E**) and strong FAP expression in tumor tissue (**F**). White arrows depict normal region resected.

**Supplemental Figure 9: Patient #007 matched  $^{68}\text{Ga}$ -FAPi-46 PET/CT and immunohistochemistry**



68-year-old female patient with verrucous squamous cell carcinoma of the right retromolar trigone who underwent right mandibulectomy (pT2 N0 M0). In correspondence of the resected lesion as shown by the yellow arrows,  $^{68}\text{Ga}$ -FAPi-46 PET/CT showed moderate uptake (**A**: Maximum Intensity Projection images (MIP), **B**: transaxial CT, **C** and **D**: transaxial PET/CT and PET, SUVmax 4.7 and SUVmean 3.9, respectively). FAP IHC on representative histologic sections demonstrated variable negative to weak FAP expression in normal tissue in an area notable for ulceration (**E**) and moderate FAP expression for tumor tissue (**F**). White arrows depict resected normal mucosa region.

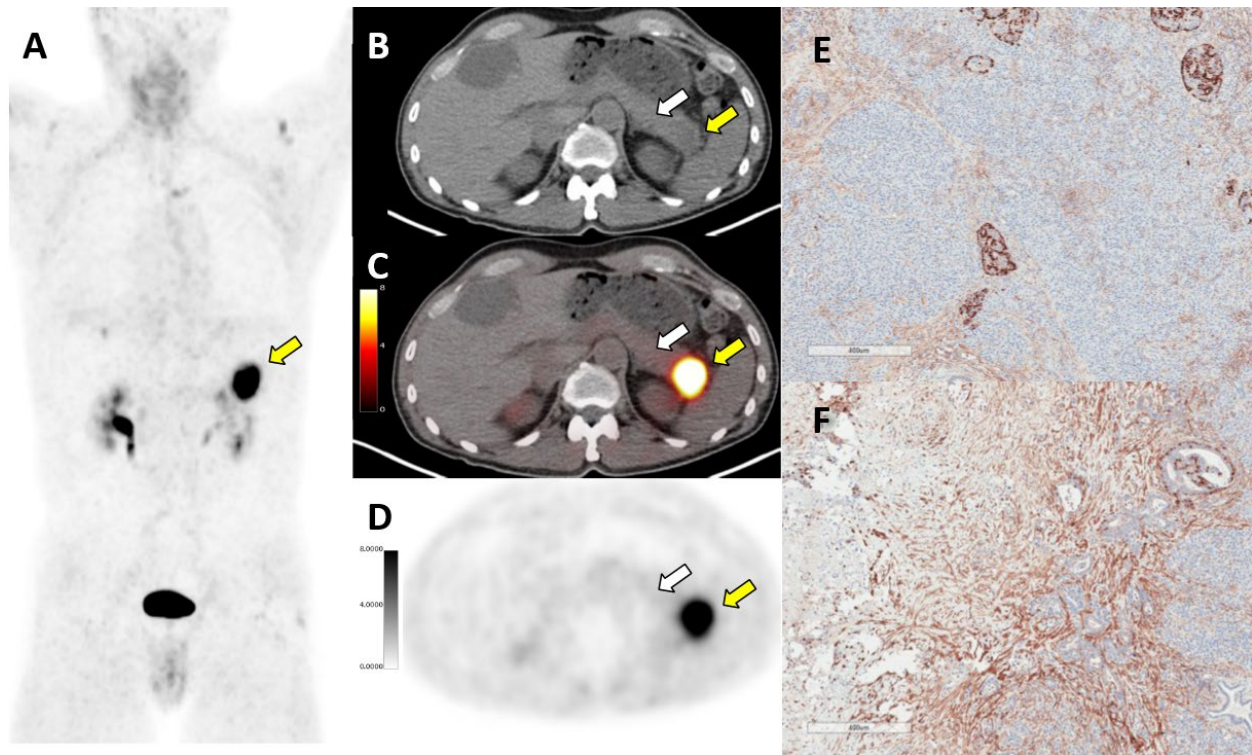
**Supplemental Figure 10: Patient #008 matched  $^{68}\text{Ga}$ -FAPi-46 PET/CT and immunohistochemistry**



36-year-old female patient with uterine squamous cell carcinoma who underwent Bilateral Salpingectomy + left pelvic lymphadenectomy (pTx N1 M0). In correspondence of the uterus lesion and the enlarged left pelvic lymph node involved by metastatic squamous cell carcinoma as shown by the yellow arrows,  $^{68}\text{Ga}$ -FAPi-46 PET/CT showed intense uptake (**A**: Maximum Intensity Projection images (MIP), **B**: transaxial CT, **C** and **D**: transaxial PET/CT and PET, SUVmax 19 and SUVmean 15.2, respectively). H&E (**E**) and FAP IHC staining (**F**) on histologic section of a representative lymph node revealed moderate to strong FAP staining of tumor cells metastasizing to the lymph node. White arrows depict resected normal contralateral lymph node.

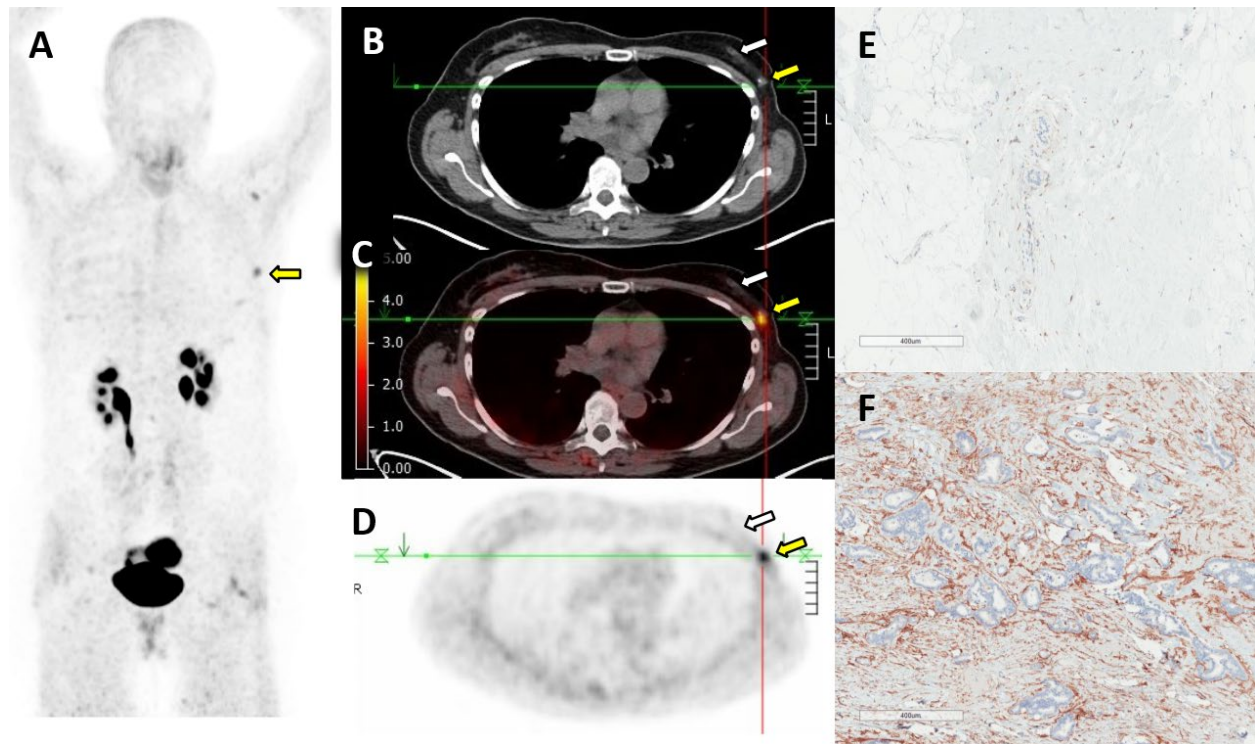


**Supplemental Figure 11: Patient #009 matched  $^{68}\text{Ga}$ -FAPi-46 PET/CT and immunohistochemistry**



65-year-old male patient with pancreatic ductal adenocarcinoma who underwent partial pancreatectomy, of the pancreatic tail (pT2 N1 M0). In correspondence of the resected lesion as shown by the yellow arrows,  $^{68}\text{Ga}$ -FAPi-46 PET/CT showed intense uptake (**A**: Maximum Intensity Projection images (MIP), **B**: transaxial CT, **C** and **D**: transaxial PET/CT and PET, SUVmax 15.7 and SUVmean 12.5, respectively). FAP IHC on representative histologic sections demonstrated variable negative to weak FAP expression in normal pancreatic parenchyma with a subpopulation of cells in normal islets consistently showing strong FAP expression (**E**). Moderate to strong FAP expression was noted for tumor tissue (**F**). White arrows depict resected normal pancreas region.

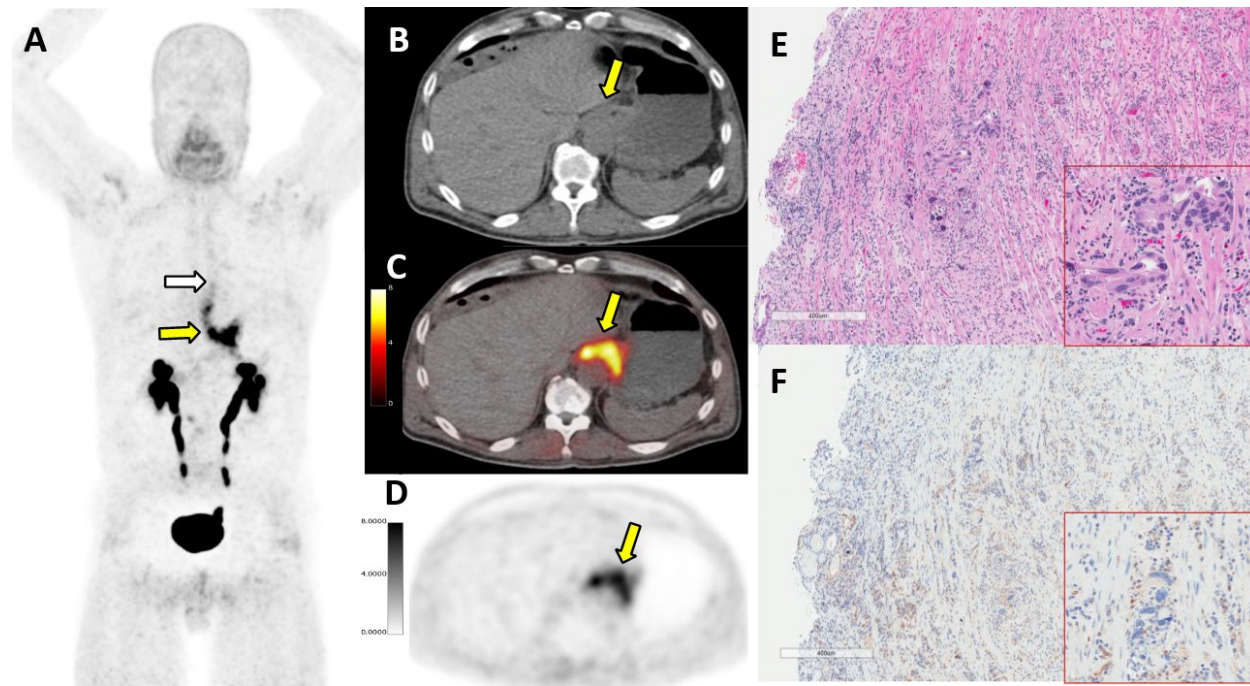
**Supplemental Figure 12: Patient #011 matched  $^{68}\text{Ga}$ -FAPi-46 PET/CT and immunohistochemistry**



65-year-old female patient with bilateral breast invasive ductal adenocarcinoma who underwent bilateral mastectomy (pT1c Nx M0). In correspondence of the resected lesion as shown by the yellow arrows,  $^{68}\text{Ga}$ -FAPi-46 PET/CT showed moderate uptake (**A**: Maximum Intensity Projection images (MIP), **B**: transaxial CT, **C** and **D**: transaxial PET/CT and PET, SUVmax 4.6 and SUVmean 4.0, respectively). FAP IHC on representative histologic sections demonstrated absent to weak FAP expression for normal tissue (**E**) and moderate to strong FAP expression for tumor tissue (**F**). White arrows depict resected normal breast region.

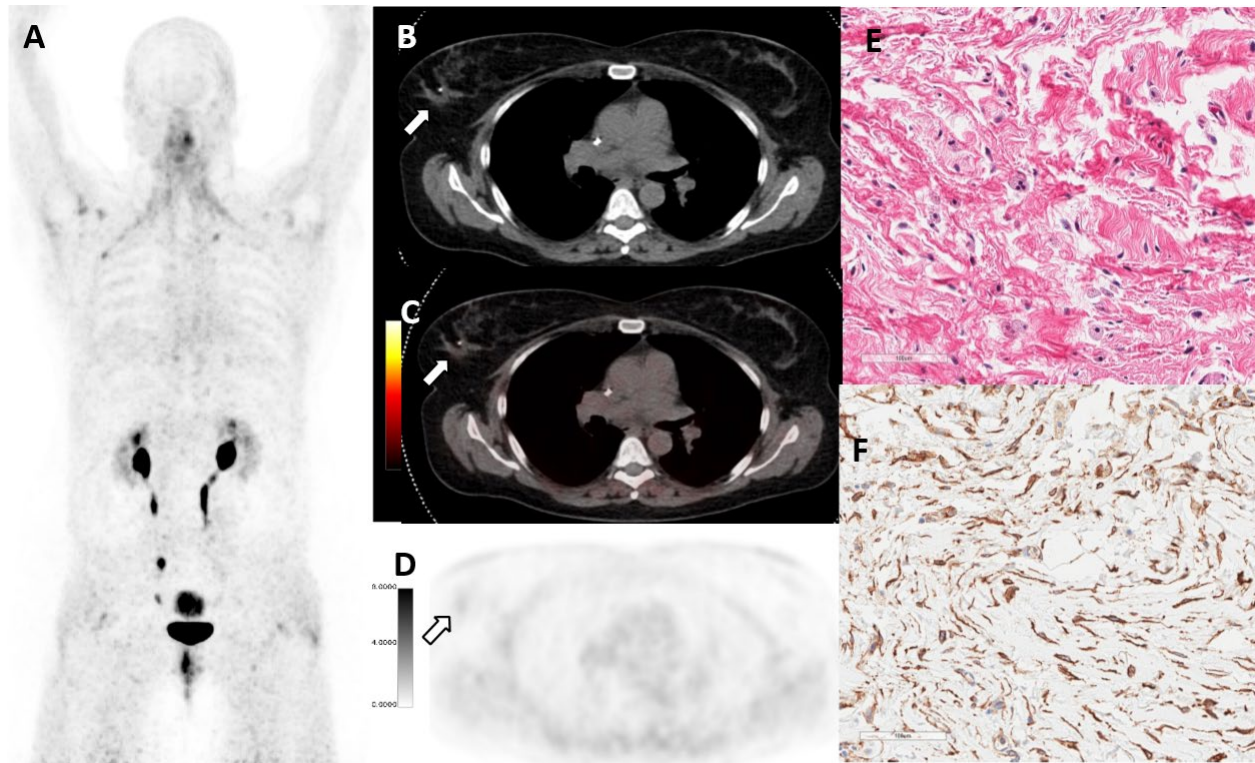


**Supplemental Figure 13: Patient #012 matched  $^{68}\text{Ga}$ -FAPi-46 PET/CT and immunohistochemistry**



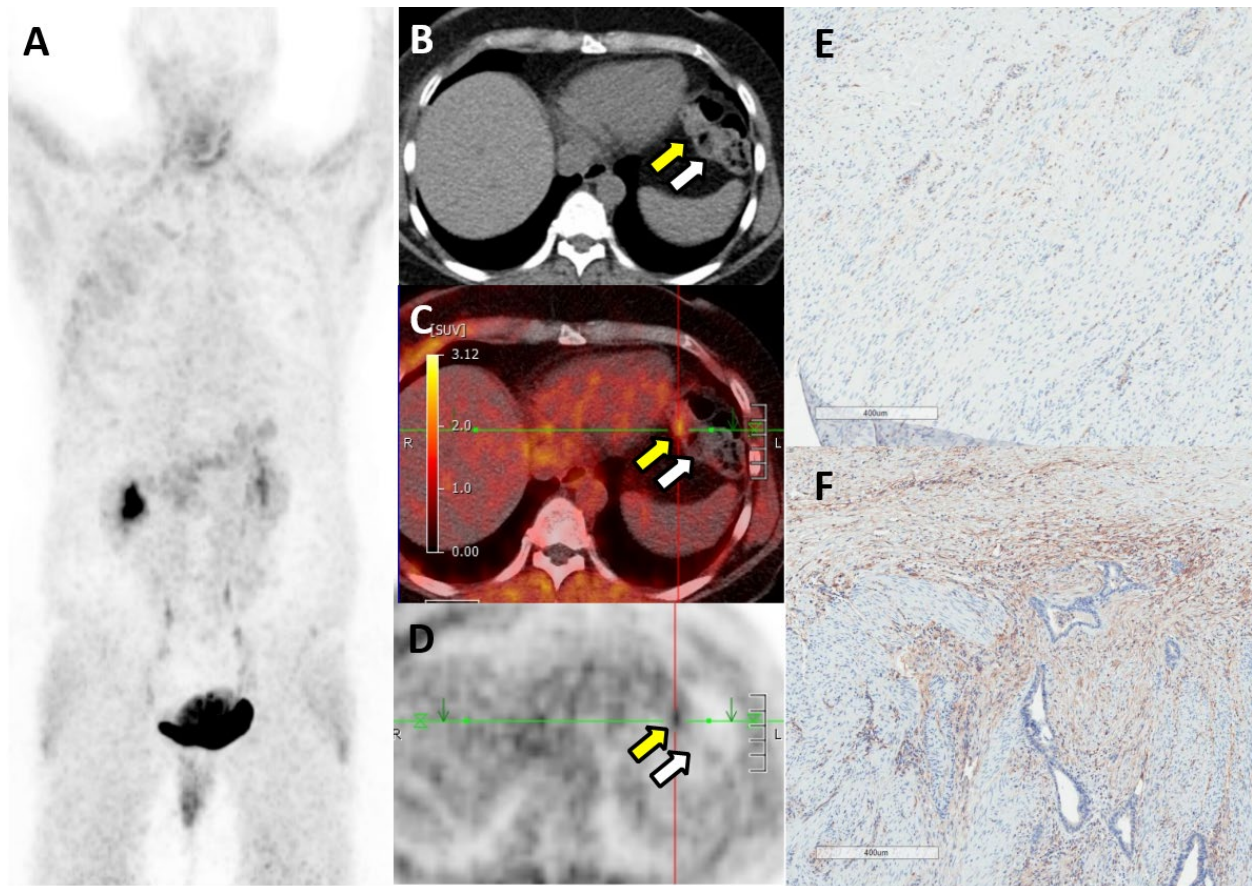
61-year-old male patient with adenocarcinoma of the gastroesophageal junction who underwent esophagogastrectomy (pT3 pN2). In correspondence of the resected lesion as shown by the yellow arrows,  $^{68}\text{Ga}$ -FAPi-46 PET/CT showed intense uptake (**A**: Maximum Intensity Projection images (MIP), **B**: transaxial CT, **C** and **D**: transaxial PET/CT and PET, SUVmax 9.1 and SUVmean 7.3, respectively). H&E (**E**) and FAP IHC staining (**F**) on histologic section of the residual small focus of adenocarcinoma revealed weak FAP staining of stroma and vessel endothelium immediately adjacent to and more distant from the tumor cells. White arrow depicts resected normal esophagus region.

**Supplemental Figure 14: Patient #013 matched PET/CT and immunohistochemistry**



51-year-old female patient with right breast invasive ductal adenocarcinoma who underwent right mastectomy and lymphadenectomy (ypT0 N0 M0). In correspondence of the resected lesion as shown by the white arrows,  $^{68}\text{Ga}$ -FAPi-46 PET/CT showed no increased uptake (**A**: Maximum Intensity Projection images (MIP), **B**: transaxial CT, **C** and **D**: transaxial PET/CT and PET, SUVmax 1.7 and SUVmean 1.4, respectively). H&E (**E**) and FAP IHC staining (**F**) demonstrated moderate FAP expression in the area of the lesion that on histologic sections revealed a complete response to neoadjuvant therapy with no residual viable tumor.

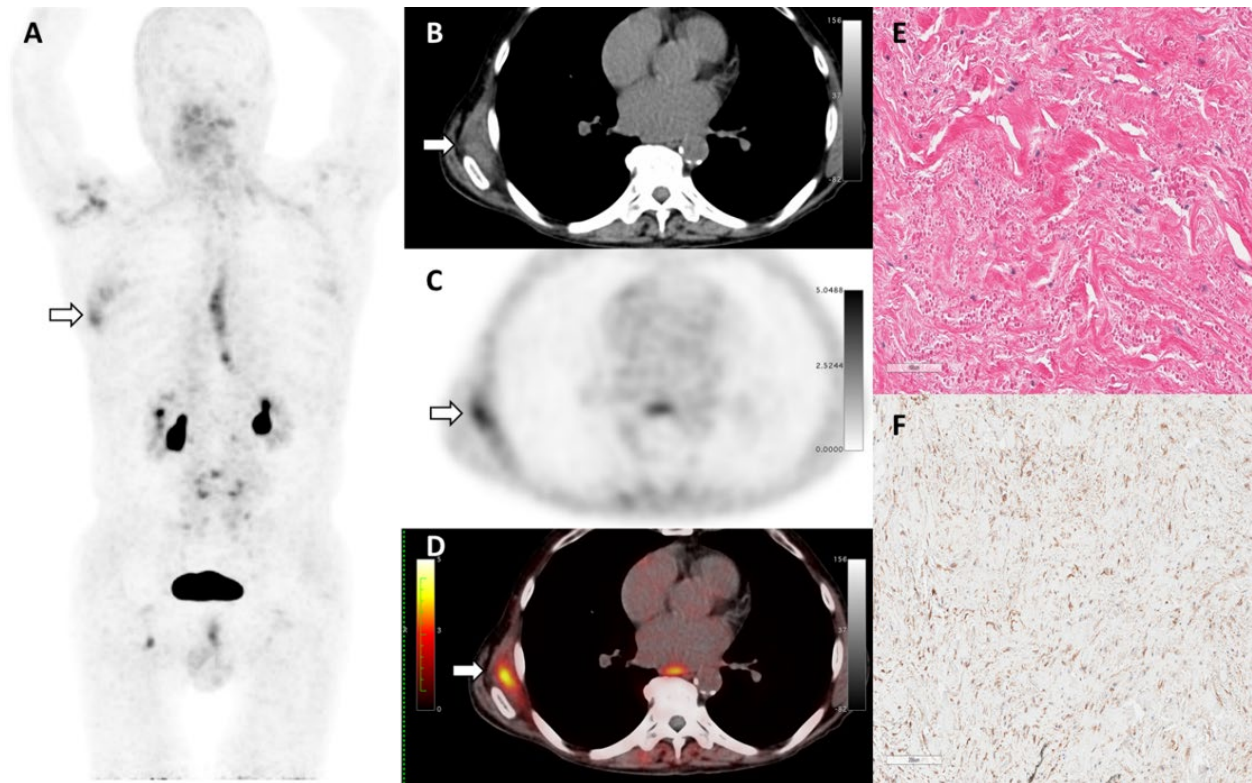
**Supplemental Figure 15: Patient #015 matched  $^{68}\text{Ga}$ -FAPi-46 PET/CT and immunohistochemistry**



56-year-old female patient with left colon adenocarcinoma with liver metastasis who underwent left hemicolectomy (ypT3 N1b M1a). In correspondence of the resected lesion as shown by the yellow arrows,  $^{68}\text{Ga}$ -FAPi-46 PET/CT showed moderate uptake (**A**: Maximum Intensity Projection images (MIP), **B**: transaxial CT, **C** and **D**: transaxial PET/CT and PET, SUVmax 2.5 and SUVmean 2.0, respectively). FAP IHC on representative histologic sections of the muscularis propria of the bowel wall demonstrated absent to weak FAP expression in vessel endothelium for normal tissue (**E**) and moderate expression for tumor tissue (**F**). White arrows depict normal region resected.



**Supplemental Figure 16: Patient #002 Elastofibroma Dorsi matched  $^{68}\text{Ga}$ -FAPi-46 PET/CT and immunohistochemistry**



A 71-year-old male patient with a right sub-scapula elastofibroma dorsi underwent  $^{68}\text{Ga}$ -FAPi-46 PET/CT. In correspondence of the resected lesion as shown by the white arrows,  $^{68}\text{Ga}$ -FAPi-46 PET/CT showed moderate diffuse increased uptake (**A**: Maximum Intensity Projection images (MIP), **B**: transaxial CT, **C** and **D**: transaxial PET/CT and PET, SUVmax 5.4 and SUVmean 4.3, respectively). H&E and FAP IHC of histologic sections of the benign elastofibroma (**E** and **F**) revealed weak FAP expression.

Full case report available PMID: 32701818 DOI: 10.1097/RLU.00000000000003218.